Document Number: AFT-2008-000056, Rev. 000(0)
PSNE Control Number: PSN-2008-0844

LONG-LIFE METALLIC FUEL FOR THE SUPER SAFE, SMALL AND SIMPLE (4S) REACTOR

Prepared by

Abdellatif M. Yacout
Nuclear Engineering Division
Argonne National Laboratory

June 2008

Toshiba Corporation

Central Research Institute of Electric Power Industry

SUMMARY

The purpose of this report is to inform the United States Nuclear Regulatory Commission of the long-life 4S metallic fuel design as part of Toshiba Corporation pre-licensing activities for the 4S reactor. The report summarizes the existing metallic fuel experience, and the associated in-pile and out-pile databases of the U-Zr based metallic fuel. Key phenomena related to the metallic fuel performance and their impacts on the current 4S fuel performance are discussed. These phenomena include fuel swelling and fission gas release, fuel constituent migration, and fuel-cladding chemical interaction. Also discussed are the run beyond cladding breach (RBCB) experience of the metallic fuel in EBR-II and the available experimental database. The implications of the characteristics of the 4S fuel design on its performance are also discussed. The main characteristics include the long fuel lifetime of 30 years and the wider and longer fuel pins compared to EBR-II and FFTF fuel pins. A review of the LIFE-METAL fuel performance code and its validation database is also included. The code is used to evaluate the performance of the 4S design. The code's analysis shows the benign nature of the design, as it enables the fuel to perform adequately during reactor operations without violating any of a conservative set of steady-state design criteria. A survey evaluation of the fuel performance is also presented. This performance bounding evaluation took into account possible fuel swelling behavior and a cladding temperature range that represent worst-case scenarios. The evaluation showed that the fuel maintains its integrity even under those worst-case conditions.

TABLE OF CONTENTS

TABLE OF CONTENTS
(Contd.)

LIST OF TABLES

LIST OF FIGURES

LIST OF FIGURES
(Contd.)

LIST OF ACRONYMS AND ABBREVIATIONS

4S	Super Safe, Small and Simple
AOO	Anticipated Operational Occurrence
BDI	bundle-duct interaction
BOL	beginning of life
CDF	cumulative damage function
CRBR	Clinch River Breeder Reactor
CRIEPI	Central Research Institute of Electric Power Industry
EBR-II	Experimental Breeder Reactor-II
EFPD	effective full-power days
FBTA	fuel behavior test apparatus
FCCI	fuel-cladding chemical interaction
FCMI	fuel-cladding mechanical interaction
FFTF	Fast Flux Test Facility
FGR	fission gas release
EOL	end of life
IC	inner core
IFR	integral fast reactor
LOFWS	loss-of-flow-without-scram
LOHSWS	loss-of-heat-sink-without-scram
MC	middle core
MOL	middle of life
MOX	mixed oxide
NRC	Nuclear Regulatory Commission
OC	outer core
PIE	post-irradiation examination
PRISM	Power Reactor Innovative Small Module
PSAR	Preliminary Safety Analysis Report
RBCB	run beyond cladding breach
RE	rare earth
SHRT	Shutdown Heat Removal Test
U.S. NRC	Unites States Nuclear Regulatory Commission
WPF	Whole-Pin-Furnace

1. INTRODUCTION

The Toshiba Corporation and Central Research Institute of Electric Power Industry (CRIEPI) has initiated the formal procedures for the licensing of the Super Safe, Small and Simple (4S) fast reactor in the United States, by providing information to the U.S. Nuclear Regulatory Commission (NRC) about the reactor's systems and fuel design. An important characteristic of the proposed fuel design is that it resides in the reactor core for the full duration of the reactor's lifetime of 30 years (no refueling) [1.1]. This long-life 4S fuel is the subject of this report, which aims at informing the NRC of the 4S fuel design characteristics and its potential for performing reliably over the full 30 years of the reactor lifetime. The 4S fuel design is based on a binary U-10wt.%Zr metallic alloy [1.2] that is clad in HT9 steel [1.3] where the use of U-10Zr metallic fuel allows for favorable thermal and safety-related characteristics (U-10Zr is used throughout the document to refer to U-10wt.%Zr). Over 16,000 binary U-10Zr fuel pins were irradiated at the Experimental Breeder Reactor-II (EBR-II) as part of the U.S. Integral Fast Reactor Program (IFR) [1.4] that extended from 1984 to 1994. Also irradiated in EBR-II during this period are more than 600 experimental U-xPu-Zr pins [1.5]. In addition, over 800 binary U-10Zr fuel pins were irradiated at the Fast Flux Test Facility (FFTF) during the late 1980s and early 1990s as part of planned conversion of the FFTF core from oxide to metallic fuel [1.6]. All irradiated pins with HT9 cladding completed their irradiation in the two reactors to high burnups up to 20 at.%, without cladding breach under normal operating conditions. The only cases of cladding failure were those induced in experimental settings to investigate certain aspects of fuel behavior, e.g., run-beyond-cladding-breach (RBCB) tests, and several failures caused by a manufacturing defect (end cap failure), which was corrected later in the program (D9 and 316 steel). This large database of irradiated binary fuel provides a sound statistical database that covers a wide range of operating conditions, and makes the case for the reliability of this fuel in fast reactor systems such as the 4S reactor.

This report starts with a description of the 4S fuel pin design and the associated irradiation parameters (Section 2). Section 3 shows the extensive size of the database upon which the 4S fuel design is based. It provides an overview of the metallic fuel experience and existing experimental database both in and outside the reactor, and summary of the different experiments conducted at EBR-II and FFTF, including both steady-state and transient experiments. Section 4 discusses the key metallic fuel phenomena that can influence fuel performance under the reactor operating conditions, including fuel swelling and axial growth, fission gas release, fuel cladding chemical interaction (FCCI), and redistribution of the fuel constituents under operating conditions. This section also includes discussion of the low-swelling HT9 cladding steel, and the RBCB behavior of the metallic fuel. The effect of those phenomena on the expected 4S fuel performance is also discussed. The LIFE-METAL metallic fuel performance code [1.7] is described in Section 5. This section also includes discussion of the code's analysis methodology, treatment of the key fuel phenomena described in Section 4, in addition to the code's validation and its applicability to the 4S fuel. The design

evaluation methodology is described in Section 6, where a set of predefined conservative design criteria is considered for the evaluation of this metallic fuel. Finally, Section 7 provides a quantitative evaluation of the performance of the 4S fuel over the 30-year lifetime using the design criteria set in Section 6 and the LIFE-METAL code. This section shows that the fuel is expected to maintain its integrity, even under bounding conditions that exceed its nominal operating conditions, and shows the viability of the current fuel design for extended use in the 4S reactor.

REFERENCES 1

1.1 Y. Tsuboi, T. Yokoyama, and N. Ueda, Trans. Am. Nucl. Soc., American Nuclear Society, **93, 41** (2005).

1.2 G. L. Hofman and L.C. Walters, in Materials Science and Technology, Vol. 10A, VCH, p. 15 (1994).

1.3 R. L. Klueh, "Elevated-Temperature Ferritic and Martensitic Steels and Their Application to Future Nuclear Reactors," ORNL/TM-2004/176, 2004, and Inter. Mater. Rev., 50 (2005) 267.

1.4 Y. I. Chang, "The Integral Fast Reactor," Nuclear Technology, **88** (1989) p. 129.

1.5 R. D. Leggett and L. C. Walters, Status of LMR Fuel Development in the United States of America, Journal of Nuclear Materials, **204**, (1993) pp. 23-32.

1.6 A. L. Pitner and R. B. Baker, Metal Fuel Test Program in the FFTF, Journal of Nuclear Materials, **204**, (1993) pp. 124-130.

1.7 M. C. Billone, Y. Y. Liu, E. E. Gruber, T. H. Hughes, and J. M. Kramer, "Status of Fuel Element Modeling Codes for Metallic Fuels," Proc. ANS International Conference on Reliable Fuels for Liquid Metal Reactors, September 7-11, 1986, p. 5-77.

2. 4S FUEL DESIGN

2.1 4S FUEL SPECIFICATIONS AND OPERATING CONDITIONS

A typical metallic fuel pin, shown in Figure 2.1, consists of a fuel slug, which is a long piece of fuel alloy that is contained (clad) in a stainless steel cladding tube, with a large plenum volume on top of the fuel slug that accommodates the release of fission gases. A sodium fill ("sodium bond") between the fuel slug and the cladding improves the heat transfer from the fuel slug to the cladding. Figure 2.2 shows a typical 4S fuel element. The proposed 4S fuel [2.1] is 2.5 meters long. It is made up of several fuel slugs stacked vertically. The plenum portion of the fuel pin is the same height as the fuel slugs (2.5 meters), the cladding material is HT9 steel [2.2], the clad thickness is 1.1 mm, and the fuel planar smeared density is 78% (the area of the fuel slug over the area of the fuel slug plus the gap area).

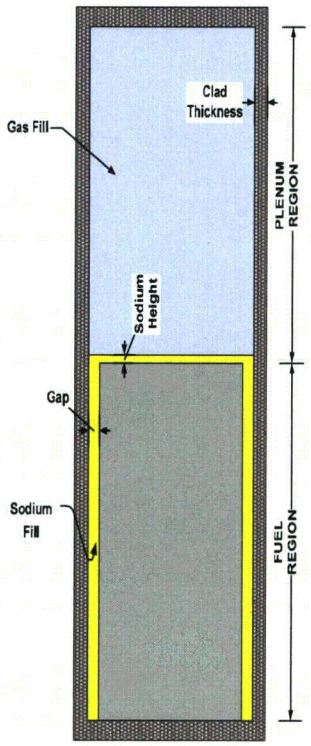

Figure 2.1. A Schematic of a Typical Metallic Fuel Pin

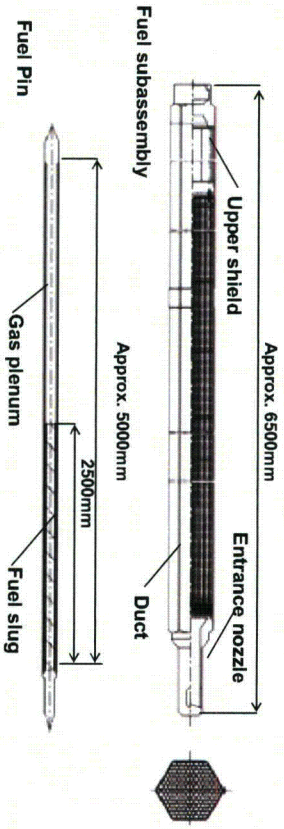

Figure 2.2. 4S Metallic Fuel Pin

The proposed 4S fuel design utilizes U-10Zr metallic alloy with two fuel enrichments of 17% and 19% U-235, in the inner and outer zones of the core, respectively, as shown in Figure 2.3. The fuel has high thermal conductivity, is compatible with sodium coolant, has sufficiently high melting temperature for safety considerations, and is well characterized through a large experimental database. This type of fuel was used as a driver fuel in EBR-II, in which over 16,000 pins were irradiated. In addition, the fuel was qualified as a driver fuel in FFTF*. Thus, a substantial history of successful operational experience with the U-10Zr fuel is available to support licensing of the 4S reactor design.

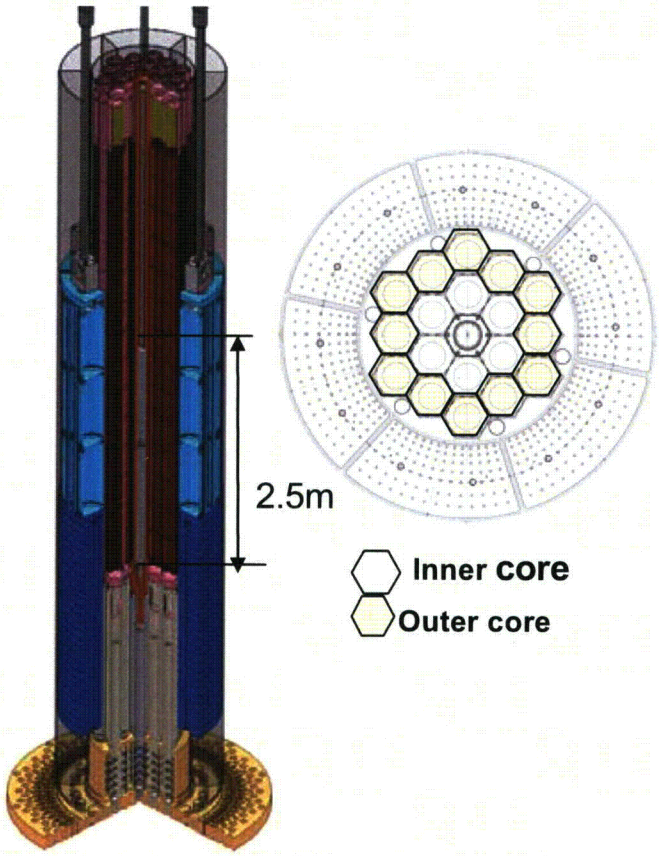

Figure 2.3. 4S Core and Fuel Enrichment Zones

* Previous comments from NRC review of the Power Reactor Innovative Small Module (PRISM) liquid metal reactor [2.3] fuel qualification plan were related to U-Zr fuel containing amounts of plutonium and minor actinides.

Table 2.1 shows the core and fuel specifications for the 4S design. The peak fast flux is $2x10^{14}$ n/cm^2-sec and the average fuel burnup is about 3.4 at.%; that is about 34,000 MWd/t, while the peak burnup is about 53,000 MWd/t. The average linear power is about 39 W/cm.

Table 2.1. Key 4S Specifications of Interest to Fuel Design

Items	Unit	Specifications/Performance
Core lifetime	year	30
Capacity factor	%	95
Electric power	MWe	10
Thermal power	MWt	30
Average burnup	GWd/t	34
Average linear power	W/cm	39
Fast neutron fluence	n/cm^2	$1.9x10^{23}$
Total neutron fluence	n/cm^2	$2.4x10^{23}$
Core height (BOL)	m	2.5
Gas plenum length	m	2.5
Inlet/outlet flow temperature	°C	355/510
U-235 enrichment (inner/outer)	%	17/19
Cladding material	-	HT9
Fuel pin diameter	mm	14.0
Fuel material	-	U-10Zr
Smeared density (BOL)	%	78
Cladding thickness	mm	1.1
Pin pitch	mm	15.1
Peak inner cladding temp (hot spot)	°C	609
No. of pins/assembly	-	169
Inner flat to flat of duct	mm	199.3
Duct thickness	mm	2.5
Duct-to-duct gap	mm	2
Duct material	-	HT9
Assembly pitch	mm	206.3

Figure 2.4 shows the power distribution over the fuel length at different stages of irradiation. The peak of the 4S distribution is located within the lower part of the fuel during a large fraction of the fuel lifetime. The implication of this characteristic will be discussed in Section 7 in relation to the possible chemical interaction between the fuel and the cladding (the highest rate of fission product generation occurs farther away from the locations of high temperature).

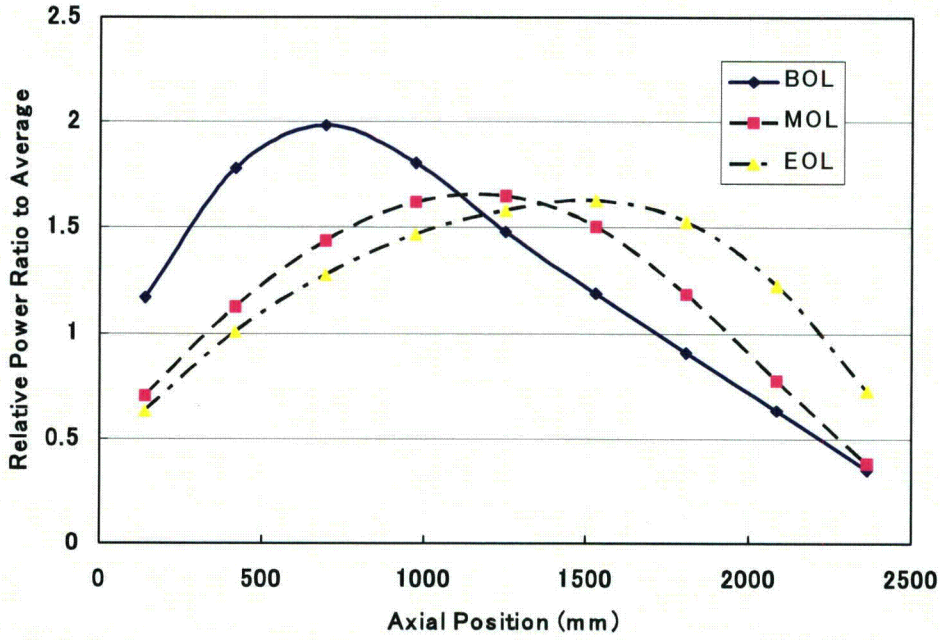

Figure 2.4. Axial Power Profile of 4S Fuel at Different Stages of Operation (BOL, MOL, and EOL are beginning, middle, and end of life, respectively.)

The burnup distribution is shown in Figure 2.5 at the end of life for the different sections of the reactor. As shown in Table 2.1, the low average burnup of about 3.4 at.% is another characteristic of the new design that will allow it to achieve the lifetime of 30 years without violating the design criteria presented in Section 7. This characteristic burnup shape of the 4S fuel burnup distribution is important to the fuel performance as it indicates lower burnup at the highest temperature location over the cladding at the top of the fuel, i.e., less than 2 at.%, which has a significant implication for fuel performance as is also discussed in Section 7.

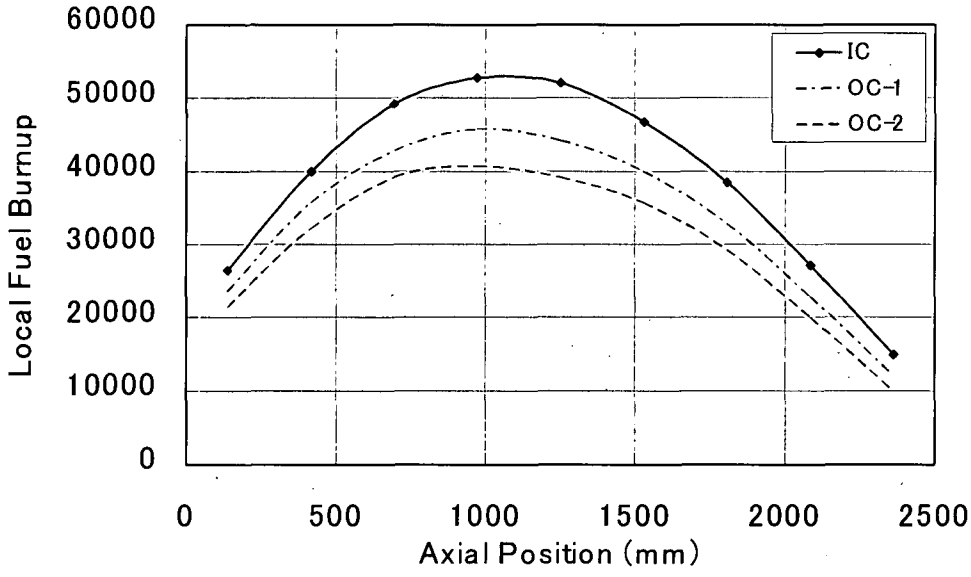

Figure 2.5. Burnup Distribution at the Fuel End of Life (IC, OC1, and OC2 are the inner, side of outer core, and corner of outer core regions, respectively.)

2.2 FUEL DESIGN PARAMETERS COMPARISON TO PREVIOUS DESIGNS

Table 2.2 provides a comparison between the 4S design parameters and the corresponding parameters in EBR-II and FFTF fuel. As shown in the table, the 4S fuel runs at a lower peak burnup than those achieved in EBR-II and FFTF. (Note that a significant number of U-10Zr fuel pins have achieved 20 at.% peak burnup without failure.) Also, the comparison shows that the 4S fuel operates at a much lower linear power, which is at least 1/5 of the range of experience in EBR-II and FFTF. Lower peak cladding temperatures, and much lower fuel center temperature and temperature gradient across the fuel, are also important 4S fuel operating characteristics. In addition, the 4S clad thickness and fuel slug diameter are approximately twice those of typical designs. The peak fast fluence is almost half of the fluence experienced for HT9 cladding (even at the higher fluence, the void swelling in HT9 is limited [2.4]). It can also be seen that the much longer 4S fuel height of 2.5 meters and much longer residence time compared to the EBR-II and FFTF designs are other characteristics of this fuel design. The 78% fuel smeared density is higher than that of typical designs (75%), but it is within the range of optimum smeared density (between 75% and 80%) that is required to achieve superior fuel performance. Details of the impact on fuel performance due to the differences between this fuel design and typical designs are discussed in Section 5.3.

Table 2.2. Comparison between 4S Key Design Parameters and the Corresponding EBR-II and FFTF Parameters

Key Parameter	EBR-II/FFTF	4S
Peak burnup, 104 MWd/t	5.0 – 20	< 5.5
Max. linear power, kW/m	33 – 50	8
Cladding hotspot temp., °C	650	609
Peak centerline temp., °C	< 700	< 630
Peak radial fuel temp. difference, °C	100 – 250	< 30
Cladding fast fluence, n/cm^2	up to 4 x 1023	2 x 1023
Cladding outer diameter, mm	4.4 – 6.9	14
Cladding thickness, mm	0.38 – 0.56	1.1
Fuel slug diameter, mm	3.33 – 4.98	10.4
Fuel length, m	0.3 (0.9 in FFTF)	2.5
Plenum/fuel volume ratio	0.84 – 1.45	1.3
Fuel residence time, years	1 – 3	30
Smeared density, %	75	78

REFERENCES 2

2.1 Y. Tsuboi, T. Yokoyama, and N. Ueda, Trans. Am. Nucl. Soc., American Nuclear Society, **93, 41** (2005).

2.2 R. L. Klueh, "Elevated-Temperature Ferritic and Martensitic Steels and Their Application to Future Nuclear Reactors," ORNL/TM-2004/176, 2004, and Inter. Mater. Rev., 50 (2005) 267.

2.3 "Preapplication Safety Evaluation Report for the Power Reactor Innovative Small Module (PRISM) Liquid-Metal Reactor," NUREG-1368.

2.4 R. D. Leggett and L. C. Walters, "Status of LMR Fuel Development in the United States of America," Journal of Nuclear Materials, **204**, (1993) pp. 23-32.1.2.

3. METALLIC FUEL EXPERIENCE AND DATABASE

A metallic U-10Zr alloy is proposed as the fuel material for the 4S reactor. In general, metal fuels consisting of uranium base alloys with Pu or alloying elements (e.g., Zr or Mo) have a number of favorable characteristics that made uranium the alloy of choice for the early fast reactors. Those characteristics include ease of fabrication, high thermal conductivity, and high fissile and fertile densities, in addition to favorable safety-related characteristics. The particular fuel experience of interest to the 4S design is that of U-Zr fuel in EBR-II and FFTF [3.1-3], in addition to out-pile tests with this alloy. Both steady-state and transient experience with this fuel are presented in the following subsections.

3.1 U-Zr FUEL EXPERIENCE

Irradiation experience with metallic fuel in EBR-II lasted for over 30 years starting in the 1960s and continued until the reactor shut down in 1994. The original EBR-II Mark-I fuel consisted of 95% uranium and 5% fissium alloy (mainly molybdenum, ruthenium, rhodium, palladium, and zirconium). The uranium-fissium Mark-II fuel with 75% smeared density and improved design replaced the 85% SD Mark-I fuel, leading to improvements in achieved burnups that reached 18.5% in some pins [3.3]. Over 40,000 Mark-II metal fuel pins have been successfully irradiated through the early 1980s.

In 1984, with the start of the Integral Fast Reactor (IFR) program, a 10 wt.% zirconium addition, replacing 5% fissium, was selected as the reference alloying agent for both uranium- and plutonium-bearing fuels. Earlier irradiation tests of various alloys indicated that Zr exhibited exceptional compatibility with cladding in addition to significantly increasing the fuel alloy solidus and fuel-cladding eutectic temperatures. Therefore, as the Mark-II driver fuel assemblies reached their irradiation limits, the EBR-II core was gradually converted to new Mark-III fuel based on U-10%Zr with D-9 or 316-SS cladding. Later, Mark-IV fuel with HT-9 cladding was introduced. In addition, U-Pu-10Zr ternary fuel was also introduced into the reactor. A total of 16,811 U-Zr fuel pins and 660 U-Pu-Zr fuel pins were irradiated in EBR-II over a period of 10 years until the reactor shut down in 1994. Burnup distributions achieved by U-Zr and U-Pu-Zr fuel pins are presented in Figures 3.1 and 3.2 [3.4]. Peak fuel pin powers reached were up to 500 W/cm. No failures were observed in any of this large number of Mark-III or Mark-IV pins under normal operating conditions. A limited number of failures were observed in experiments where the operating conditions were intentionally altered from normal conditions. Those failed pins were either operating under temperatures that are much higher than normal operating temperatures (experiment X447 [3.5]), or operating with reduced cladding, to check the fuel behavior beyond cladding breach (RBCB) [3.6]).

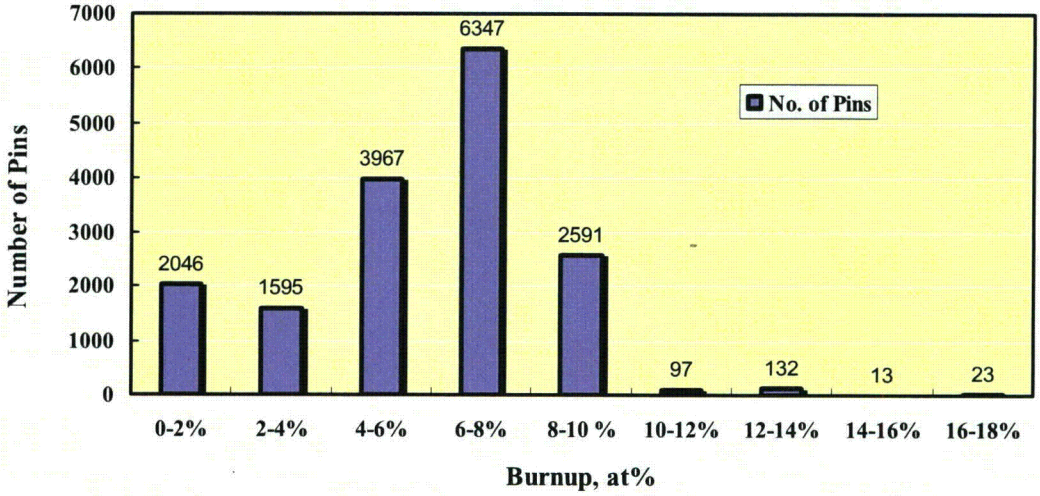

Figure 3.1. Burnup Distribution of U-Zr Fuel Pins in EBR-II (Ref. 4.2)

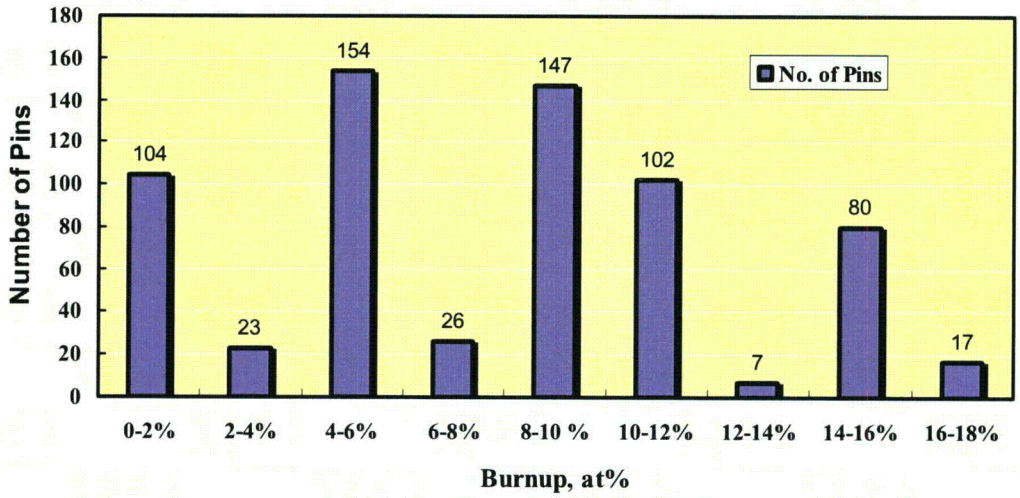

Figure 3.2. Burnup Distribution of U-Pu-Zr Fuel Pins in EBR-II (Ref. 4.2)

In addition to the 30 years of extensive irradiation experience in EBR-II, eight full assemblies of metallic fuel were irradiated in FFTF [3.2, 3.7]. One assembly, "IFR-1," contained 37 U-Pu-Zr fuel pins and 132 U-10Zr fuel pins; all have D9 cladding and achieved a peak burnup of 10 at.%. The other assemblies were part of the core conversion qualification tests of U-Zr fuel with HT-9 cladding, and contained more than

800 pins. All these assemblies achieved peak burnups in excess of 10 at.% and the lead test achieved a peak burnup of 16 at.%. No failures were observed in any of the metallic fuel pins irradiated in FFTF, where many of those pins were irradiated under operating conditions that were substantially more aggressive than those of EBR-II irradiation conditions.

The extensive experimental program conducted at EBR-II and FFTF during the IFR program is summarized in Table 3.1. [3.8]. The experiments examined the effects of different phenomena that impact the fuel lifetime such as fuel swelling, fission gas release, and fuel-cladding chemical interaction. In addition, the experiments assessed the performance of different advanced steel alloys such as the 20% cold-worked austenitic D9 and the ferritic-martensitic HT9 as future duct and cladding materials with improved swelling and irradiation creep behavior. Other experiments considered variations in the fuel alloy composition, including Zr contents higher or lower than 10 wt.%, or variations in Pu content. Experiments that included variations in the fuel and cladding dimensions considered wider fuel slugs, longer effective fuel length, and different smeared densities. Ultimately, the experimental program has proved the viability of the U-Zr fuel and its excellent performance up to high burnups. The steady-state irradiation database of EBR-II experiments shown in Table 3.1 includes post-irradiation examination (PIE) results from those experiments, combined with detailed operating conditions of the experiments and all the subassemblies in EBR-II since the start of the IFR program. Operating conditions for some of the experiments were estimated in great detail and were used to analyze the results of the PIE [3.9, 3.10]. The physics-related operating conditions such as the fluence and linear powers are stored in a detailed physics database [3.11].

Table 3.1. Summary of Main Metal Fuel Experiments at EBR-II and FFTF [3.8]

Experiment Number	Fuel Composition	Cladding Material	No. of Rods in Assembly	Smeared Density (%)	Cladding OD (cm)	Wall Thickness (cm)	Plenum/Fuel Vol. Ratio	Peak Power (kW/m) (beginning of life)	Peak Cladding Temp. (°C) (beginning of life)	Peak Burnup (at.%)	Fast Fluence x10*22n/cm^2 (E>0.1MeV)	Key Breached Rod Information
X419 Prototype & fuel behavior	U-10Zr, U-8Pu-10Zr, U-19Pu-10Zr	D9	61	75	0.584	0.038	1	39.4	560	11.9	12	
X420 Prototype, fuel behavior, failure mode, RBCB	U-10Zr, U-8Pu-10Zr, U-19Pu-10Zr	D9	61	75	0.584	0.038	1	36.1	590	18.4	18.5	1 breach @ 16.4 at.% burnup; 530°C at breach
X421 Prototype, fuel behavior, failure mode	U-10Zr, U-8Pu-10Zr, U-19Pu-10Zr	D9	61	75	0.584	0.038	1	39.4	560	17.1	19.6	
X423 Fuel swelling & restructuring	U-10Zr, U-3Pu-10Zr, U-8Pu-10Zr, U-19Pu-10Zr, U-22Pu-10Zr, U-26Pu-10Zr	316	37	75	0.737		1	42.7	522	4.9	8.07	

Table 3.1. Summary of Main Metal Fuel Experiments at EBR-II and FFTF [3.8] (Contd.)

Experiment Number	Fuel Composition	Cladding Material	No. of Rods in Assembly	Smeared Density (%)	Cladding OD (cm)	Wall Thickness (cm)	Plenum/Fuel Vol. Ratio	Peak Power (kW/m) (beginning of life)	Peak Cladding Temp. (°C) (beginning of life)	Peak Burnup (at%)	Fast Fluence x10*22n/cm^2 (E>0.1MeV)	Key Breached Rod Information
X425 (X425A/B/C) Lead IFR	U-10Zr, U-8Pu-10Zr, U-19Pu-10Zr	HT9	61	75	0.584	0.038	1	48.2	590	3,11,16.2, 19.3	20.6	
X429 (X429A/B) Fabrication variables & strain prediction	U-10Zr, U-8Pu-10Zr, U-19Pu-10Zr	HT9, 316SS	61	75	0.584	0.038	1	42.7	600	7.7,10.6, 14.4	13.8	1 breach @ 6.5 at.% burnup & 1 breach @ 10 at.% burnup
X430 (X430A/B) HT9, peak cladding temp., large diameter, compatibility	U-10Zr, U-19Pu-10Zr, U-22Pu-10Zr, U-26Pu-10Zr	HT9	37	75	0.737	0.041	1.4	49.2	540	11.5	20.6	
X431 (X431A) Blanket safety	U-2Zr, U-6Zr, U-10Zr	HT9	19	85	0.940	0.038-0.051	1.8	39.4	507	3.9	15.4	

Table 3.1. Summary of Main Metal Fuel Experiments at EBR-II and FFTF [3.8] (Contd.)

Experiment Number	Fuel Composition	Cladding Material	No. of Rods in Assembly	Smeared Density (%)	Cladding OD (cm)	Wall Thickness (cm)	Plenum/Fuel Vol. Ratio	Peak Power (kW/m) (beginning of life)	Peak Cladding Temp. (°C) (beginning of life)	Peak Burnup (at%)	Fast Fluence x10*22n/cm^2 (E>0.1MeV)	Key Breached Rod Information
X432 (X432A) Blanket safety	U-2Zr, U-6Zr, U-10Zr	HT9	19	85	0.940	0.038-0.051	1.8	39.4	507	4.5	16.6	
X435 (X435A) Mk-III qual.	U-10Zr	D9	61	75	0.584	0.038	1.4	49.2	591	19.8	22.8	
X436 Mk-III qual.	U-10Zr	D9	61	75	0.584	0.038	1.4	34.4	596		8.45	
X437 Mk-III qual.	U-10Zr	D9	61	75	0.584	0.038	1.4	37.7	597		10	
X438 Mk-III qual.	U-10Zr	D9	61	75	0.584	0.038	1.4	32.8	623		9.45	
X441 (X441A) Design parameters	U-10Pu -6, 10, 12Zr	HT9 D9	61	70, 75, 85	0.584	0.038-0.048	1.0, 1.5, 2.1	49.2	600	12.7	10.1	
X447 (X447A) U-Zr high-temp.	U-10Zr	HT9	49	75	0.584	0.046	1.4	36.1	660	10	9.17	2 breaches @ 9.5 at% burnup; 630°C at breach

Table 3.1. Summary of Main Metal Fuel Experiments at EBR-II and FFTF [3.8] (Contd.)

Experiment Number	Fuel Composition	Cladding Material	No. of Rods in Assembly	Smeared Density (%)	Cladding OD (cm)	Wall Thickness (cm)	Plenum/Fuel Vol. Ratio	Peak Power (kW/m) (beginning of life)	Peak Cladding Temp. (°C) (beginning of life)	Peak Burnup (at%)	Fast Fluence x10*22n/cm^2 (E>0.1MeV)	Key Breached Rod Information
X448 (X448A) Mk-IV qual.	U-10Zr	HT9	61	75	0.584	0.046	1.4	45.9	552	14.6	14.9	
X449 Mk-IV qual.	U-10Zr	HT9	61	75	0.584	0.046	1.4	29.5	578	11.3	17.7	
X450 Mk-IV qual.		HT9	61	75	0.584	0.046	1.4	36.1	576	10.2	13.1	
X451 (X451A) Mk-IV qual.	U-10Zr	HT9	61	75	0.584	0.046	1.4	32.8	623	13.7	13.7	
X452 Fuel impurities	U-10Zr	D9	61	75	0.584	0.038		34.4	596	6.1	5.38	
X453 Fuel impurities	U-10Zr	D9	61	75	0.584	0.038		34.4	596	8.5	8.45	
X454 Fuel impurities	U-10Zr	D9	61	75	0.584	0.038		49.2	547	8.3	9.12	
X455 Fuel impurities	U-10Zr	D9	61	75	0.584	0.038		49.2	547	10.3	9.16	

Table 3.1. Summary of Main Metal Fuel Experiments at EBR-II and FFTF [3.8] (Contd.)

Experiment Number	Fuel Composition	Cladding Material	No. of Rods in Assembly	Smeared Density (%)	Cladding OD (cm)	Wall Thickness (cm)	Plenum/Fuel Vol. Ratio	Peak Power (kW/m) (beginning of life)	Peak Cladding Temp. (°C) (beginning of life)	Peak Burnup (at%)	Fast Fluence x10*22n/cm^2 (E>0.1MeV)	Key Breached Rod Information
X483 (X483A) Mk-IIIA, reference 316SS qual.	U-10Zr	316	61	75	0.584	0.038	1.4	49.9	552	14.8	15.7	
X484 Mk-IIIA, reference 316SS qual.	U-10Zr	316	61	75	0.584	0.038	1.4	36.1	576	11.7	11.9	
X485 Mk-IIIA, reference 316SS qual.	U-10Zr	316	61	75	0.584	0.038	1.4	39.7	576	10.5	10.7	
X486 Mk-IIIA, reference 316SS qual.	U-10Zr	316	61	75	0.584	0.038	1.4	37.1	623	13.9	13.9	
X489 High-Pu for PRISM design	U-19Pu-10Zr, U-28Pu-10Zr	HT9, HT9M	61	75	0.584	0.046	1.4	36.1	606	5.4	4.83	

Table 3.1. Summary of Main Metal Fuel Experiments at EBR-II and FFTF [3.8] (Contd.)

Experiment Number	Fuel Composition	Cladding Material	No. of Rods in Assembly	Smeared Density (%)	Cladding OD (cm)	Wall Thickness (cm)	Plenum/Fuel Vol. Ratio	Peak Power (kW/m) (beginning of life)	Peak Cladding Temp. (°C) (beginning of life)	Peak Burnup (at%)	Fast Fluence x10*22n/cm^2 (E>0.1MeV)	Key Breached Rod Information
X492 (X492A/B) Zr-sheathed fuel	U-3Zr, U-20.5Pu-3Zr	HT9, HT9M	61	75	0.584	0.038	1.4	41.0	551	10.5	11.1	
X496 Long lifetime	U-10Zr	HT9	37	59	0.686	0.056	3	63.3	536	8.3	6.9	
X501 Minor-actinide-bearing fuel	U-20.2Pu-10Zr-1.3Np-1.2Am, U-10Zr	HT9	2+59	75	0.584	0.046	1.4	44.9	≤540	7.6	6.4	
IFR-1 Fuel column length effects	U-10Zr, U-8Pu-10Zr, U-19Pu-10Zr	D9	169	75	0.686	0.056	1.2	49.2	615(604)	94 GWd/MTHM	15.4	
MFF1A FFTF lead metal fuel test	U-10Zr	HT9	8	75	0.686	0.056	1.2	42.7	577	38 GWd/MTHM	5.6	

Table 3.1. Summary of Main Metal Fuel Experiments at EBR-II and FFTF [3.8]
(Contd.)

Experiment Number	Fuel Composition	Cladding Material	No. of Rods in Assembly	Smeared Density (%)	Cladding OD (cm)	Wall Thickness (cm)	Plenum/Fuel Vol. Ratio	Peak Power (kW/m) (beginning of life)	Peak Cladding Temp. (°C) (beginning of life)	Peak Burnup (at%)	Fast Fluence x10*22n/cm^2 (E>0.1MeV)	Key Breached Rod Information
MFF-1 FFTF lead metal fuel test	U-10Zr	HT9	5	75	0.686	0.056	1.2	43.0	577	95 GWd/MTHM	17.3	
MFF-2 FFTF metal prototype	U-10Zr	HT9	169	75	0.686	0.056	1.3	54.1	618	143 GWd/MTHM	19.9	
MFF-3 FFTF metal prototype	U-10Zr	HT9	169	75	0.686	0.056	1.3	59.1	643	138 GWd/MTHM	19.2	
MFF-4 FFTF Series III.b qualification	U-10Zr	HT9	169	75	0.686	0.056	1.5	56.8	618	135 GWd/MTHM	19	
MFF-5 FFTF Series III.b qualification	U-10Zr	HT9	169	75	0.686	0.056	1.5	55.8	651	101 GWd/MTHM	14	

Table 3.1. Summary of Main Metal Fuel Experiments at EBR-II and FFTF [3.8]
(Contd.)

Experiment Number	Fuel Composition	Cladding Material	No. of Rods in Assembly	Smeared Density (%)	Cladding OD (cm)	Wall Thickness (cm)	Plenum/Fuel Vol. Ratio	Peak Power (kW/m) (beginning of life)	Peak Cladding Temp. (°C) (beginning of life)	Peak Burnup (at%)	Fast Fluence x10*22n/cm^2 (E>0.1MeV)	Key Breached Rod Information
MFF-6 FFTF Series III.b qualification	U-10Zr	HT9	169	75	0.686	0.056	1.5	55.8	588	141 GWd/MTHM	12.8	

3.2 CLADDING BREACH

As mentioned previously, more than 16,000 metallic U-Zr fuel pins have been irradiated in EBR-II and FFTF. No pin failure was observed in pins clad in HT9 steel (similar to the 4S fuel) at normal operating conditions. A total of about 22 pins of other types of cladding breached, of which 16 breached in defective welds (due to a welding problem early in the program that was corrected), 3 breached in the plenum region due to unknown causes, and 3 breached in the fuel column region due to creep failure of the D9 cladding [3.8]. The first of the fuel column breaches occurred in a D9-clad, U-Pu-Zr rod in assembly X420B, the second reconstitution of the IFR lead assembly X420, at 16.4 at.% burnup. The breach occurred about 2/3 up the height of the fuel column at an area where rod-rod interaction was expected to be the highest, suggesting that cladding interaction with the fuel and/or with an adjacent rod played a role in the cladding breach, which is not an issue for the 4S low-swelling HT9 cladding. Two breaches occurred in the X429A and X429B assemblies, reconstitutions of the fabrication variables experiment, at 6.5 and 10 at.% burnup, where, in both cases, the fabrication parameters are altered (e.g., high smeared density). The only failures occurring in an HT9-clad U-Zr pins were at about 9.5 at.% burnup in assembly X447A, which was orificed to operate at a higher-than-nominal cladding temperature [3.5].

3.3 RUN BEYOND CLADDING BREACH (RBCB)

The behavior of fuel pins after a breach during operation is of particular importance for the 4S design because of the long fuel residence time and the non-refueling core feature of the reactor. Thus, it is possible that a limited number of breached pins will be allowed to continue operating after breach without replacement for the remainder of the reactor life. The benign nature of the RBCB behavior of metallic fuel will allow such behavior without major release of any significant amount of fuel material into the coolant or propagation of a pin failure to other pins. In addition to the breaches taking place during normal operation, mentioned in the previous subsection, seven other fuel pins were intentionally altered to cause failure shortly after placement in reactor. These pins were the subject of RBCB experiments [3.6, 3.12]. The experiments are summarized in Table 3.2 [3.8]. The experiments were conducted in EBR-II using pre-irradiated fuel pins with defects machined into the cladding so that breach would take place shortly after placement in reactor. After breach, the reactor continued operations with the breached fuel pins to allow assessment of post-breach behavior. Four of the breached fuel rods contained U-Fs, U-Zr, or U-Pu-Zr fuel clad in Type 316 stainless steel in experimental assemblies XY-21A, XY-24, and XY-27. Three breaches occurred in U-Zr and U-Pu-Zr rods clad in D9 and HT9 stainless steels within assemblies X482, X482A, and X482B, which were tests intended to operate with breached fuel. Another naturally breached fuel rod in assembly X420B was also maintained under irradiation for some time after breach for the same purpose.

Table 3.2. Summary of Run-Beyond-Cladding-Breach (RBCB) Metallic Fuel Experiments in EBR-II (Refs. 3.6, 3.8, 3.12)

Test Designation	Test Type	No. Rods	Fuel Composition	Cladding Type	Cladding OD (cm)	Pitch-to-Diameter Ratio	Linear Power[d] (kW/m)	Cladding Temp. (°C)	Burnup[e] (at.%)	No. Rods Breached	Days Irr'd after Breach
XY-21	BFTF[a]	1, 60[b]	U-5Fs	316SS	0.44	1.38	24	573	7.9	0	N/A
XY-21A	BFTF	1, 60[b]	U-5Fs	316SS	0.44	1.38	25	593	9.3	1	54
XY-24	FPTF[c]	2, 59[b]	U-19Pu-10Zr	316SS	0.44	1.38	21	541	7.6	1	233
XY-27	BFTF	2, 59[b]	U-8Pu-10Zr	316SS	0.44	1.38	23	520	~6.0	2	131
X482	Open Core	1, 60[b]	U-19Pu-10Zr	D9	0.58	1.24	39	600	14.4	1	168
X482A	Open Core	1, 60[b]	U-10Zr	D9	0.58	1.24	36	600	13.5	1	100
X482B	Open Core	1, 60[b]	U-19Pu-10Zr	HT9	0.58	1.24	36	600	~14	1	150
X420B	Natural Breach	61	U-19Pu-10Zr	D9	0.58	1.24	-	-	~17	1	34

a. BFTF: Breached Fuel Test Facility in EBR-II, which provided separate delayed neutron signal monitoring for the experiment and an above-core sampler for collection of released fuel and contamination.
b. First number indicates the number of pre-defected (thinned) rods, and the second number indicates the remaining number of rods in the assembly. Note that the XY-series tests used instrumented assemblies that contained 61 Mark-II-size EBR-II rods, which would typically fill a 91-pin EBR-II Mark-II driver assembly.
c. FPTF: Fission Product Test Facility in EBR-II with provision for monitoring fission products released from a breached fuel rod.
d. Linear power values for metal fuel tests are pre-test predictions.
e. Burnup values for metal fuel tests are burnup at end of test.

The analysis of the results of the RBCB experiments confirmed the benign post-breach behavior of the metallic fuel [3.6, 3.12]. A key characteristic of the metallic fuel is that it is compatible with the sodium coolant and no chemical interaction between the fuel and coolant takes place, eliminating the possibility of the formation of reaction products. Such products could further stress the breach crack or escape through the cladding into the coolant. Post-test examination indicated that mass loss from the fueled metal pins was due to expulsion of bond sodium, fission gas, and cesium, and no further fission products were released to the coolant. The release of fission gas reduced the source of stress for post-breach widening of the crack, although it was found that with lower-swelling HT9 cladding, the closer cladding proximity to the fuel could allow cracks to be subsequently widened by fuel/cladding mechanical interaction (FCMI). However, this is not a concern for the 4S fuel with HT9 cladding, since the low burnup of the fuel precludes the possibility of FCMI and the possible enlargement of the cracks. The amount of fuel washed out of the breached fuel pins was small, and any observed widening of the breach due to fuel swelling was inconsequential, as there was no fuel extruded through the crack. These results indicate that a fast reactor with metallic fuel in general, and particularly low-burnup 4S fuel, can operate with breached fuel without disrupting the reactor operations.

As mentioned before, the 4S reactor is expected to be able to operate if necessary with breached fuel until the end of the fuel life, which is the same as the reactor lifetime. However, only a total of 30 breached fuel elements, representing less than 1% of the core, will be allowed to limit the possible radiation exposure consequences. Beyond this 1% fraction, an action to replace the failed fuel will have to be taken.

3.4 FUEL FABRICATION EXPERIENCE

There is a large mount of experience with fabricating metallic fuel in the U.S., in particular at the facilities associated with EBR-II. The fuel pins fabricated included about 90,000 Mark-I/IA driver fuel pins [3.13], over 30,000 Mark-II driver fuel pins [3.14], and more than 16,000 Mark-III/IIIA/IV (U-10Zr alloy) driver fuel pins in addition to more than 600 U-Pu-Zr pins. The experience included the use of 316 stainless steel, D9, and HT9 as cladding material. Over the years, fuel manufacturing specifications became well defined and are based on well known manufacturing procedures. Those specifications and procedures will be used to fabricate the 4S fuel.

3.5 EXPERIENCE WITH GRID SPACERS

Although grid spacers have been widely used in thermal reactors to support the fuel pins within a subassembly, there is limited experience with their use in fast reactors. Instead, the majority of fast reactor fuel experience is associated with the use of wire wraps. One example of that limited experience is the testing of three grid-spaced subassemblies in FFTF [3.15]. Those test subassemblies performed satisfactorily for 3 and 4 FFTF cycles reaching 85,000-96,000 MWd/t (oxide fueled subassemblies) and peak fast fluence of 1.3x1023 n/cm^2. The performance was similar to that of wire wrapped subassemblies.

The fretting wear from flow vibration due to use of grid spacer is expected to be small due to low flow velocity and large pin stiffness comparing to FFTF fuel.

3.6 TRANSIENT AND OFF-NORMAL OPERATION EXPERIENCE

A wide range of data is available for different in-pile and out-of-pile transient tests with metallic fuel, in addition to off-normal reactor operations that test the fuel under extreme conditions. In-reactor transient tests were performed at EBR-II for both Mk-II U-Fs driver fuel and Mk-IIIA U-Zr fuel [3.12, 3.16]. These tests evaluated the effects of the transients on the fuel lifetime, and qualified the driver fuel for transient operation. Tests were performed at different rates of power increase (low-ramp-rate and high ramp rates); some of the test subassemblies contained driver fuel that was exposed to previous transients and some were operating at high temperatures. Evaluation of the test results found no indication of fuel failure or significant degradation of the metal driver fuel even in the extreme temperature exposure cases [3.12]. Although these tests were completed with U-Fs Mark-II fuel, the results were extended to U-10Zr (Mark-IIIA) driver fuel, which underwent EBR-II transient-overpower tests during and after the core conversion from Mark-II to Mark-IIIA driver fuel.

Passive safety tests were conducted in EBR-II and were designated the Shutdown Heat Removal Tests (SHRT) [3.17]. The tests demonstrated the ability of a metal-fueled fast reactor to withstand loss-of-flow-without-scram (LOFWS) events and loss-of-heat-sink-without-scram events (LOHSWS) with no core damage. In conjunction with these tests, a high-temperature test was conducted to assess the damage the transients would cause to the EBR-II driver fuel and to qualify the fuel for transient operation [3.12, 3.18, 3.19].

Tests simulating extreme off-normal conditions, designated the M-series tests, were conducted at the Transient Reactor Test Facility (TREAT). The six M-series tests evaluated transient-overpower margin to failure, pre-failure axial fuel expansion, and post-failure fuel and coolant behavior for 15 pins with various combinations of U-5Fs, U-Zr, and U-Pu-Zr fuel clad in Type 316, D9, and HT9 stainless steel [3.20, 3.21]. The results consistently showed that metal fuel pins of modern design exhibited failure thresholds of around four times nominal power (under the relatively fast transient-overpower conditions used in the tests). The data from these tests and from a large number of previous metal fuel transient tests in TREAT were used to develop and validate models of fuel behavior under transient overpower conditions [3.22, 3.23, 24].

Other safety-related testing focused on fuel behavior during unlikely loss-of-flow events, using hot-cell furnace heating tests of irradiated U-Pu-Zr clad in HT9 [3.23, 3.24, 3.26]. The results demonstrated significant safety margin for the particular transient conditions studied (a bounding unlikely loss-of-flow event for EBR-II). The observed cladding breaches were induced by pin-plenum gas pressure at temperature, with

cladding thinning due to eutectic-like formation of a molten phase at the fuel/cladding interface. In addition, fission gas expansion in the fuel induced axial fuel expansion, enabled by reduction of constraint from the cladding with the formation of the molten phase at the fuel/cladding interface. The data from these tests, and other similar tests, were used to develop and validate models of fuel behavior under loss-of-flow conditions [3.23, 3.24, 3.25].

REFERENCES 3

3.1 R. D. Leggett and L. C. Walters, "Status of LMR Fuel Development in the United States of America," Journal of Nuclear Materials, **204**, (1993) pp. 23-32.1.2.

3.2 C. Lam et al., "Experience with Advanced Driver Fuels in EBR-II," Journal of Nuclear Materials, 204, (1993) 119-123.

3.3 A. L. Pitner and R. B. Baker, "Metal Fuel Test Program in FFTF," Journal of Nuclear Materials, 204, (1993) 124-130.

3.4 Small Modular Fast Reactor Design Description, ANL-SMFR-1, 2005.

3.5 R. G. Pahl, D. L. Porter, D. C. Crawford, and L. C. Walters, "Irradiation Behavior of Metallic Fast Reactor Fuels," Journal of Nuclear Materials, **188**, (1992) pp. 3-9.

3.6 G. L. Batte and G. L. Hofman, "Run-Beyond-Cladding-Breach (RBCB) Test Results for the Integral Fast Reactor (IFR) Metallic Fuels Program," Proceedings of International Fast Reactor Safety Meeting 1990. Snowbird, Utah: American Nuclear Society, La Grange Park, IL.

3.7 H. Tsi and L. A. Neimark, "Irradiation Performance of Full-Length Metallic IFR Fuels," Proc. Int. Conf. on Design and Safety of Advanced Nuclear Power Plants, October 25-29 1992, Tokyo, Japan.

3.8 D. C. Crawford, D. L. Porter, S. L. Hayes, "Fuels for Sodium-Cooled Fast Reactors: US perspective," Journal of Nuclear Materials, 371, (2007) 202 231.

3.9 A. M. Yacout, S. Salvatores, and Y. Orechwa, "Degradation Analysis Estimates of the Time-to-Failure Distribution of Irradiated Fuel Elements," *Nucl. Tech.*, 113, 177 (1996).

3.10 A. M. Yacout, W. S. Yang, G. L. Hofman, and Y. Orechwa, "Average Irradiation Temperature for the Analysis of In-Pile Integral Measurements," *Nucl. Tech.*, 115, 61 (1996).

3.11 A. M. Yacout, S. Salvatores, and Y. Orechwa, "Database for Analysis of Advanced Reactors Fuel and Cladding Materials," *Trans. Am. Nucl. Soc.*, 69, 193 (1993).

3.12 B. R. Seidel, G. L. Batte, N. E. Dodds, G. L. Hofman, C. E. Lahm, R. G. Pahl, D. L. Porter, H. Tsai, and L. C. Walters, "A Decade of Advances in Metallic Fuel in LMR: A Decade of LMR Progress and Promise," Nov 11-15 1990. Washington, D.C.: American Nuclear Society, La Grange Park, IL.

3.13 L. C. Walters and J. H. Kittel, "Development and Performance of Metal Fuel Elements for Fast Breeder Reactors," Nuclear Technology, **48**, (1980) p. 273.

3.14 R. E. Einziger and B. R. Seidel, "Irradiation Performance of Metallic Driver Fuel in Experimental Breeder Reactor II to High Burnup," Nuclear Technology, **50**, (1980) pp. 25-39.

3.15 P. J. Levine, G. W. Schulze, T. P. Soffa and A. Boltax, "Grid-Spaced and Wire-Wrapped Fuel Assembly Tests in FFTF," Proceedings of the International Conference on Reliable Fuels for Liquid Metal Reactors, Tucson, AZ, (September 1986), pg. 3-92.

3.16 R. D. Leggett and L. C. Walters, "Status of LMR Fuel Development in the United States of America," Journal of Nuclear Materials, **204**, (1993) pp. 23-32.

3.17 G. H. Golden, H. P. Planchon, J. I. Sackett, and R. M. Singer, "Evolution of Thermal-Hydraulics Testing in EBR-II," Nuclear Engineering and Design, **101**, (1987) pp. 3-12.

3.18 C. E. Lahm, J. F. Koenig, P. R. Betten, J. H. Bottcher, W. K. Lehto, and B. R. Seidel, "EBR-II Driver Fuel Qualification for Loss-of-Flow and Loss-of-the-Heat-Sink Test without SCRAM," Nuclear Engineering and Design, 101, (1987) pp. 25-34.

3.19 C. E. Lahm, J. J. Koenig, and B. R. Seidel, "Consequences of Metallic Fuel-Cladding Liquid Phase Attack During Over-Temperature Transient on Fuel Element Lifetime," Proceedings of International Fast Reactor Safety Meeting. 1990. Snowbird, Utah: American Nuclear Society, La Grange Park, IL.

3.20 T. H. Bauer, A. E. Wright, W. R. Robinson, J. W. Holland, and E. A. Rhodes, "Behavior of Modern Metallic Fuel in TREAT Transient Overpower Tests," Nuclear Technology, **92**, (1990) pp. 325-352.

3.21 A. E. Wright, D. S. Dutt, and L. J. Harrison, "Fast Reactor Safety Testing in TREAT in the 1990s," International Fast Reactor Safety Meeting. 1990. Snowbird, Utah: American Nuclear Society, La Grange Park, IL.

3.22 K. J. Miles, "Metal Fuel Safety Performance," Proceedings of the International Topical Meeting in Safety of Next Generation Fast Reactors, May 1-5, 1988. Seattle, WA: American Nuclear Society, La Grange Park, IL.

3.23 J. M. Kramer, Y. Y. Liu, M. C. Billone, and H. C. Tsai, "Modeling the Behavior of Metallic Fast Reactor Fuels During Extended Transients," Journal of Nuclear Materials, **204**, (1993) pp. 203-211.

3.24 Y. Y. Liu, H. Tsai, M. C. Billone, J. W. Holland, and J. M. Kramer, "Behavior of EBR-II Mk-V-Type Fuel Elements in Simulated Loss-of-Flow Tests," Journal of Nuclear Materials, **204**, (1993) pp. 194-202.

3.25 T. Sofu, J. M. Kramer, and J. E. Cahalan, "SASSYS/SAS4A-FPIN2 Liquid-Metal Reactor Transient Analysis Code System for Mechanical Analysis of Metallic Fuel Elements," Nuclear Technology, 113, (1996) pp. 268-279.

3.26 H. Tsai, Y. Liu, A. Smith, N. Gupta, and S. Bellamy, "Potential Eutectic Failure Mechanism for Stainless Steel Cans Containing Plutonium Metal," Proc. 15th Inter. Symposium on the Packaging and Transportation of Radioactive Materials, PATRAM 2007, October 21-26, 2007, Miami, Florida, pg. 1-14.

4. PHENOMENA AFFECTING METALLIC FUEL PERFORMANCE

Reference [4.1] is a comprehensive overview of the metallic fuel behavior and phenomena associated with its use in fast reactors. In particular, the reference discusses in detail the phenomena associated with the U-Zr based fuel in fast reactors that are of interest to the 4S fuel design. This section provides an overview of those phenomena and discusses their relation to the expected performance of the 4S fuel. The phenomena of interest include swelling and fission gas release in metallic fuel, fuel constituent redistribution, and fuel-cladding chemical interaction.

4.1 SWELLING AND FISSION GAS RELEASE

Fuel swelling is driven by nucleation and growth of immobile fission-gas bubbles (mainly Xe and Kr). The accumulated release of fission gas from the fuel leads to pressurization of the fuel plenum. This gas pressure is the primary loading mechanism on the cladding, in addition to possible loading from FCMI. During irradiation, those insoluble fission gases are released and accumulate within the fuel until a release path from the fuel is created at sufficient burnups. In metal fuel, this path is formed through the interlinkage of porosity within the fuel. As shown in Figure 4.1, the fraction of fission gases that are released from the fuel increases rapidly with burnup as the fraction of porosity within the fuel increases with fuel swelling. The correlation of fission gas release with swelling appears to be independent of fuel alloy as shown in Figure 4.2. Initially, both the volumetric swelling and fission gas release increase rapidly with burnup. As the fuel comes in contact with the cladding, the rate of increase is reduced as shown in Figure 4.1.

The key design feature that enables this swelling and fission gas release profile is the choice of fuel planar smeared density. A choice of an optimal smeared density between 75% and 80% will allow sufficient planar swelling, up to 30%, to facilitate fission gas release from the fuel to the plenum before the fuel comes in contact with the cladding. The continuous release of a large fraction of the fission gases to the plenum by the time the fuel comes in contact with the cladding reduces the potential for FCMI stresses on the cladding. Given this optimum smeared density, the FCM stresses become effective only at high burnups (e.g., 10 at.% or more) due to the accumulation of solid fission products within the fuel. The 4S fuel design is based on 78% smeared density. At this smeared density, the fuel swelling behavior will be consistent with the previous designs and, given the low average burnup of the fuel of about 3.4 at.%, the potential for FCMI stress on the cladding is eliminated. Also, it is important to point out here that given this fuel smeared density, the fuel is expected to come in contact with the cladding after 1.5-2 at.% burnup. This is expected to limit the effects of FCCI at the top region of the cladding where the clad temperature is the highest. In this region, the EOL burnup is lower than 2 at.% and the fuel is expected to come in contact with the cladding for only a small fraction of the fuel lifetime or not at all.

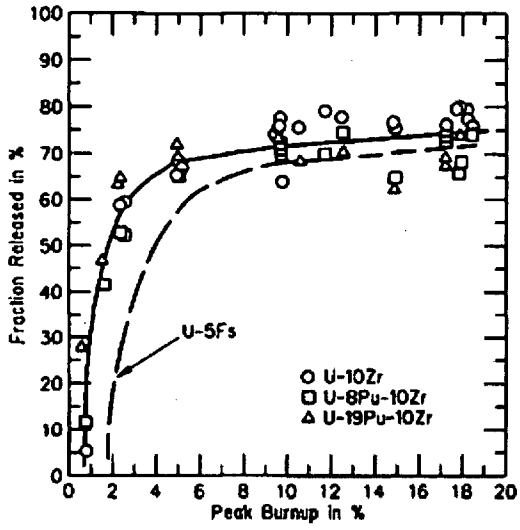

Figure 4.1. Fission Gas Release vs. Burnup for Different Types of Metallic Fuel

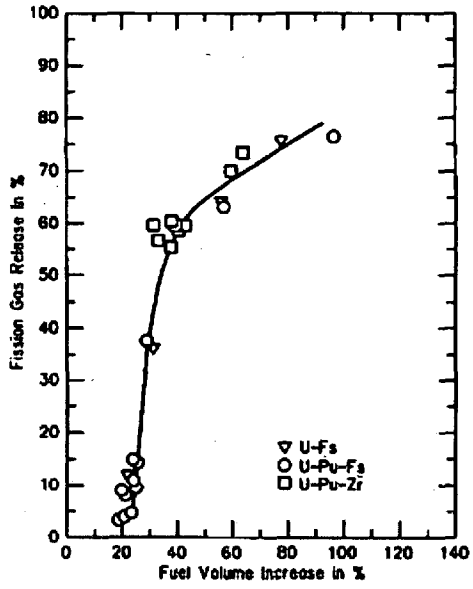

Figure 4.2. Fission Gas Release vs. Swelling

As for the gas release mentioned before, 75% fuel planar smeared density allows sufficient planar swelling, approximately 30%. This much planar swelling would, for isotropic swelling, translate to a length increase of approximately 15%. However, the observed length increases are consistently smaller, indicating anisotropic swelling as shown in Figure 4.3. The main reason for this effect appears to be the difference in swelling behavior between the hotter center of the fuel pin and the colder periphery [4.2]. In the center part of the fuel, γ-phase predominates, and the α-phase dominates in the peripheral zone. The two phases have different swelling characteristics, which leads to the anisotropic fuel swelling. A large anisotropy can be associated with the presence of Pu in the fuel as shown in Figure 4.3. This anisotropy is due to a change in the various alloy phases present in the fuel radial zones associated with rapid radial Zr redistribution in the radial direction as will be discussed in the following section.

In the case of the 4S reactor, the fuel temperature is lower than the fuel temperature of the typical fuel irradiated at EBR-II or FFTF, as it is expected to be much lower than 700°C (peak hot channel inner clad temperature is about 609°C and the temperature drop across the fuel is expected to be less than 100°C). At such low fuel temperatures, the dominant phase across the fuel cross-section is expected to be the α phase as shown in the U-Zr phase diagram in Figure 4.4. The implication of such a phase distribution within the 4S fuel is that the swelling behavior of the fuel is expected to be isotropic, which puts the axial growth of the fuel in the upper range of existing experience (~ 10%).

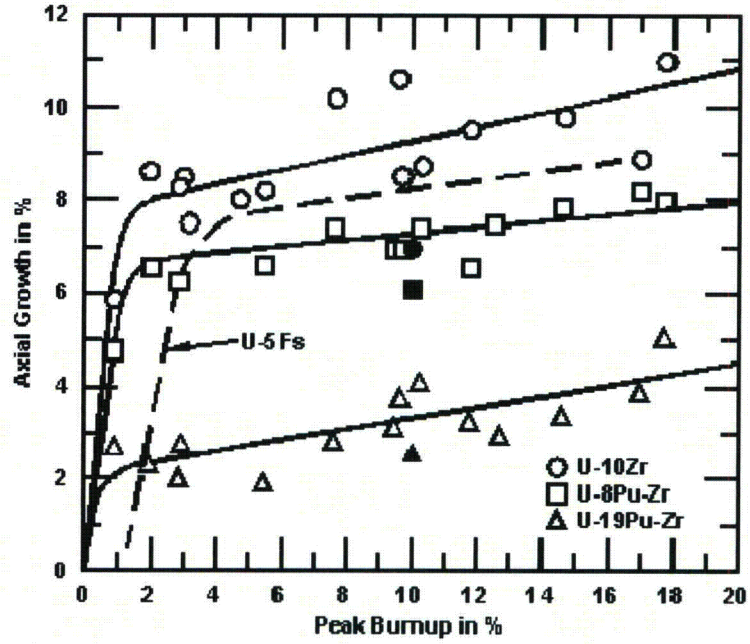

Figure 4.3. EBR-II Fuel Length Increase in Various Metallic Fuels as a Function of Burnup (Closed symbols correspond to FFTF data [4.3].)

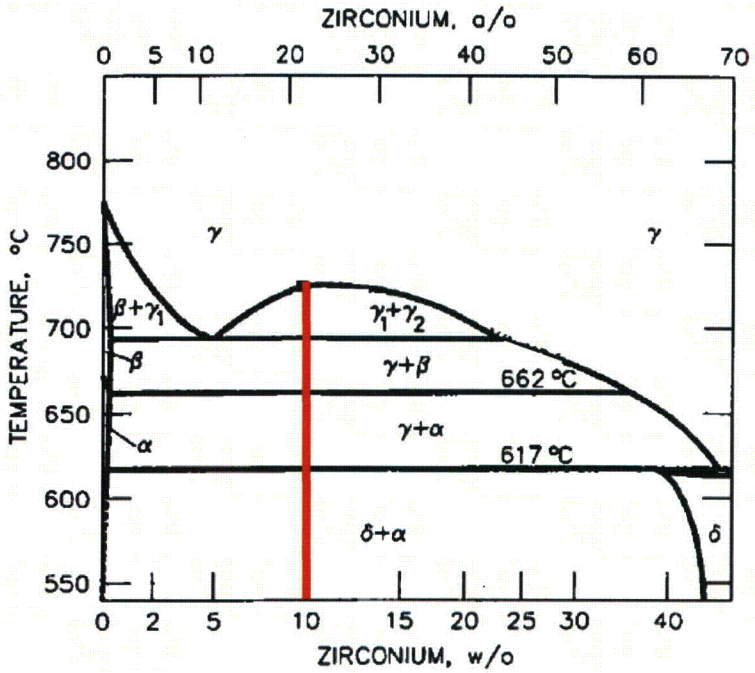

Figure 4.4. U-Zr Phase Diagram

Finally, PIE of U-10Zr pins in the IFR-1 experiment at FFTF [4.3] showed axial growth that is consistent with the high growth of this alloy, although the growth is less than that observed in EBR-II for U-10Zr by about 1-2% (about 7% after 10 at.% burnup). Although PIE has not been performed on the other full-length U-10Zr fuel irradiated in FFTF, the MFF series, information from the FFTF instrumentation tree provided a clue to the extent of the axial growth in those subassemblies [4.4]. These instruments measured the reduction in subassembly outlet flow temperatures during the first several weeks of irradiation. This drop in temperature cannot be explained by the fuel depletion effect, but was a result of the axial growth of the fuel in the test subassemblies out of the active core region. As shown in Figure 4.5, the observed decrease in coolant temperature change through the assembly exceeded 3%, which can be correlated to about 7% axial growth. This growth rate is consistent with the IFR-1 results, and as shown in the figure, the axial growth saturates after about 60 effective full-power days (EFPD) or about 1.5% burnup.

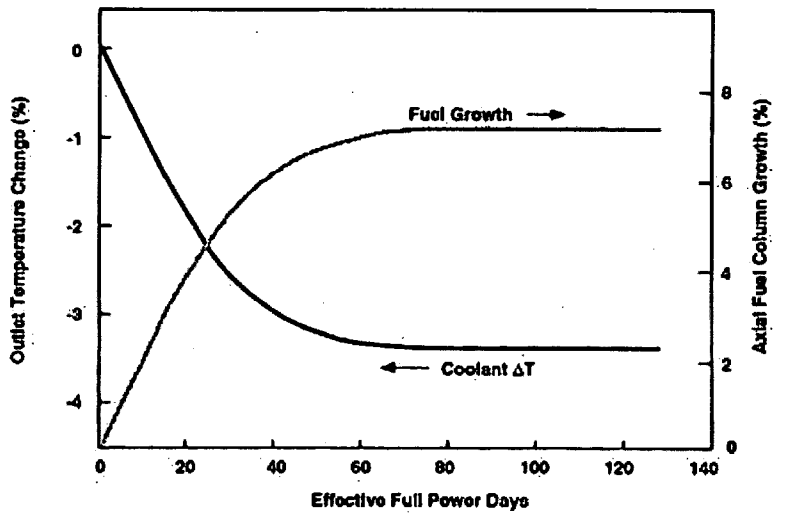

Figure 4.5. Axial Fuel Growth Effects Observed in Metal Fuel Tests at FFTF (Ref. 4.4)

4.2 CONSTITUENT REDISTRIBUTION

Constituent redistribution in a metallic U-Zr/U-Pu-Zr alloy fuel is a commonly observed irradiation phenomenon, which was first reported in the 1960s. As shown in Figure 4.6, the microstructures of the irradiated fuels exhibit three distinct concentric zones. The zones are a Zr-enriched central zone, a Zr-depleted and U-enriched intermediate zone, and a slightly Zr-enriched zone on the outer periphery (the presence of Pu > 8% enhances the redistribution of U and Zr [4.2]). Notice the temperature dependence of the redistribution in Figure 4.6, where a wider redistribution middle ring is formed at the top of the fuel compared to the lower part. The annular zone structure is also characterized by distinct differences in porosity. The migration of Zr atoms is understood to be caused by the radial temperature gradients in the fuel temperature range

encompassing a multi-phase regime in which each phase field has different thermochemical properties. Although there are some irregularities, in general the U profile is opposite of that of Zr.

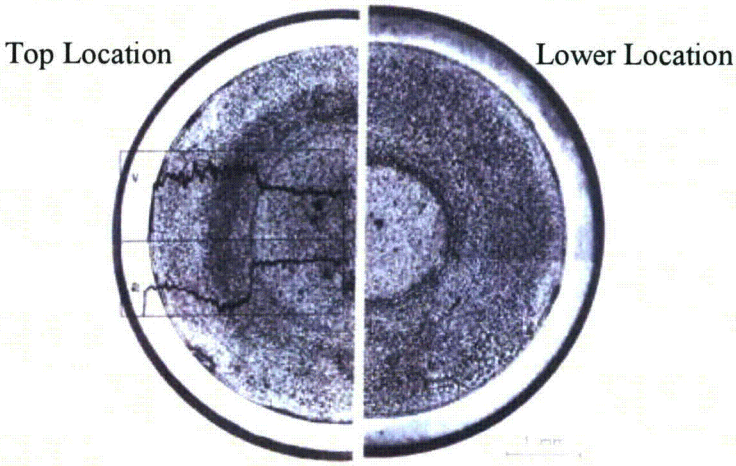

Figure 4.6. U-10Zr at 10 at.% BU (DP-11 from X447 at different axial locations)

There are a number of performance-degrading issues associated with this phenomenon. The reduction of Zr fraction in areas within the fuel reduces the fuel melting point within those regions and potentially reduces the power to melt during accident sequences. During normal operations, the temperature drop across the fuel is low (usually < 200°C), as a result of the high thermal conductivity of the metal fuel, and the temperature drop across the fuel-cladding gap is negligible due to the presence of the sodium bond. This leads to a peak fuel temperature that is dictated by the limit on inner clad temperature, which is dependent on the type of cladding. For example, HT9 ferritic-martensitic steel has limited thermal creep properties that impose a nominal steady-state inner clad temperature that is less than 620°C. This leads to peak fuel temperatures that are far from the melting temperature even in regions where the Zr is depleted.

A more significant effect of redistribution is its impact on the fuel swelling rates and axial fuel growth. As mentioned before, the multiphase regimes present across the fuel radius, due to the redistribution phenomenon, have different growth rates that are believed to play a part in observed metal fuel anisotropic growth [4.1].

Analysis of the axial growth of the 4S fuel based on the expected fuel swelling and the possible lock-up effects is provided in [4.5]. (Lock-up effect is the reduction or elimination of fuel axial growth due to friction as the fuel comes in contact with the cladding.) The possible impacts of redistribution on fuel axial growth and fuel-cladding lock-up effects are discussed. Figure 4.7 shows the results of the time to gap closure analysis, which determines the amount of axial swelling. Case 1 represents a varying

power profile during irradiation, while case 2 shows the results for a fixed power profile, which is the average of the three profiles in Figure 2.4. The results of the analysis predict no radial redistribution of Zr and isotropic 4S fuel axial growth that can lead to about 9.7% axial growth (Case 1) taking into account the lock-up effects.

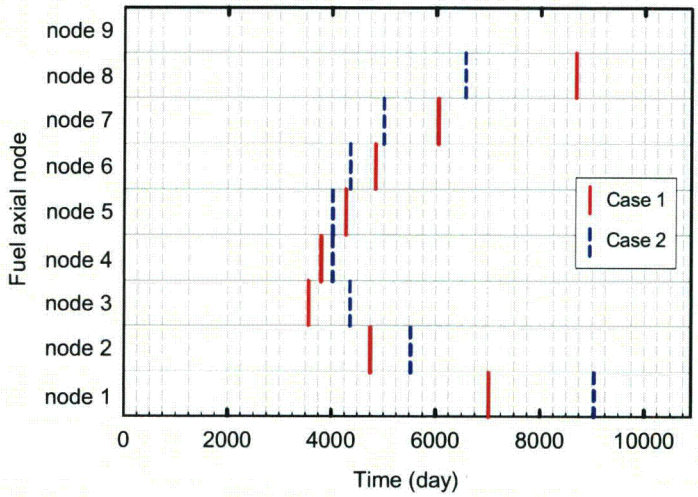

Figure 4.7. Time to Gap Closure at Each Axial Node Marked by a Vertical Line for Two 4S Fuel Design Cases

4.3 FUEL-CLADDING CHEMICAL INTERACTION (FCCI)

FCCI, as shown in Figure 4.8, when interdiffusion between the fuel and cladding components takes place, represents a two-fold potential problem for metallic fuel. It both weakens the cladding mechanical properties and leads to the formation of relatively low melting point compositions in the fuel. During normal operations, FCCI is characterized by solid-state interdiffusion, although a liquid phase may form during transient temperatures of 700-800°C. In general, FCCI in metallic fuel can be characterized by two stages of interaction as shown in Figure 4.9, where the different possible cladding wastage mechanisms are indicated. Prior to accumulation of lanthanide fission products at the fuel-cladding interface (due to fission product migration), FCCI is characterized by a ferritic layer formation. This layer can be a result of Ni depletion in austenitic cladding or decarburization of the martensitic cladding. This type of interaction has time and temperature dependence characteristic of solid-state diffusion.

Ultimately, lanthanides control FCCI as they migrate to the fuel-cladding interface with amounts that are functions of both burnup and extent of radial migration in the fuel. This radial migration increases with both fuel temperature and the presence of Pu in the fuel.

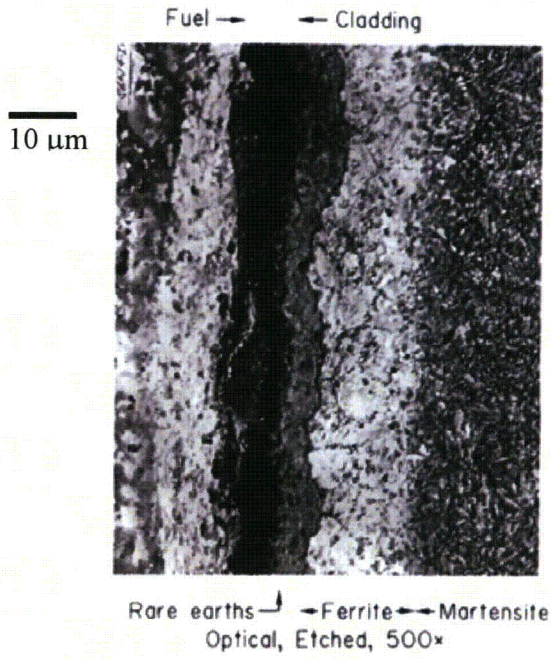

Figure 4.8. Fuel-Cladding Interdiffusion of U-10Zr and HT-9, in Pile, after 6 at.% Burnup at ~ 620°C

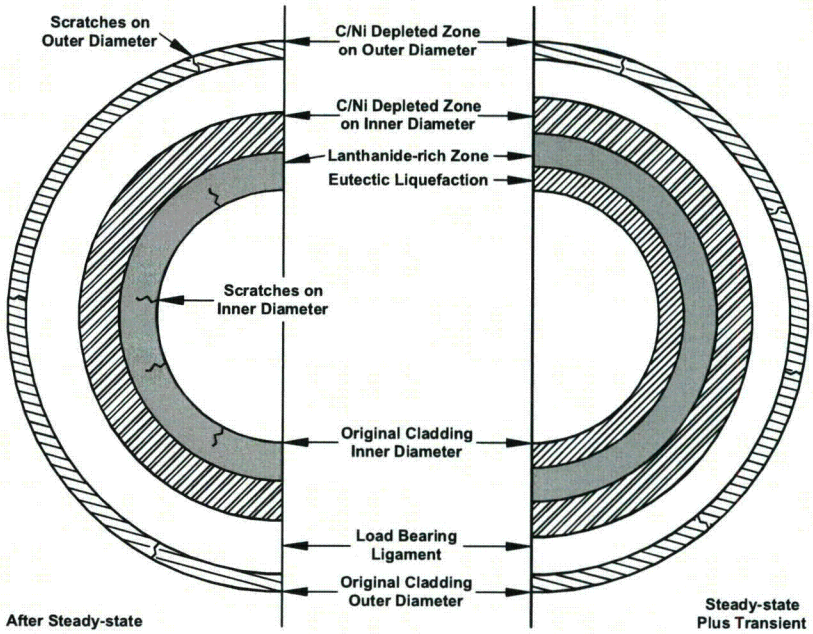

Figure 4.9. Cladding Wastage Mechanisms

REFERENCES 4

4.1 G. L. Hofman and L. C. Walters, Chapter 1, "Metallic Fast Reactor Fuels," in "Material Science and Technology, A Comprehensive Treatment," Volume 10A, Edited by R. W. Cahn, P. Haasen and E. J. Kramer, 1994.

4.2 G. L. Hofman, R. G. Pahl, C E. Lam, D. L. Porter, *Met. Trans. A. 21A*, 517.

4.3 H. Tsai and L. A. Neimark, "Irradiation Performance of Full-Length Metallic IFR Fuels," Proceedings of the International Conference on Design and Safety of Advanced Nuclear Power Plants (ANP'92), Vol. III, 23.2-1, 1992.

4.4 A. L. Pitner and R. B. Baker, "Metal Fuel Test Program in FFTF," Journal of Nuclear Materials, 204, (1993) 124-130.

4.5 Y. S. Kim, A. M. Yacout, G. L. Hofman, and H. J. Ryu, Trans. Am. Nucl. Soc., Vol. 96, p. 709, 2007.

5. LIFE-METAL FUEL PERFORMANCE CODE

The LIFE-METAL [5.1] fuel performance code has been developed to predict the behavior of metallic fuel pins. The code has evolved from the LIFE series of codes that perform steady-state and design-basis-transient analyses for the thermal, mechanical, and radiation behavior of nuclear fuel pins [5.2]. The LIFE-4CN code [5.3], which forms the basis for LIFE-METAL, includes two fuel options [(U, Pu)C and (U, Pu)N], two fuel/cladding thermal-bond options (He and Na), numerous cladding options (e.g., solution-annealed and 20% cold-work Type-316 stainless steels, HT9, etc.), and one coolant option (Na). A detailed thermomechanical analysis is performed in the radial direction with provisions to specify up to 20 radial rings for the fuel/cladding system. Axial variations in operating conditions are accounted for by inputting powers and fast fluxes for up to nine fuel axial nodes and one plenum node. Thermally, the axial nodes are coupled through the calculated coolant temperatures. However, axial heat conduction is ignored (a good approximation), and there are no provisions for mechanical coupling between axial nodes. The following sections describe the code's general analysis methodology, and its validation to experimental data. A detailed discussion of the code's applicability to the evaluation of the 4S fuel is also included.

5.1. ANALYSIS METHODOLOGY

A detailed mechanical analysis is performed for both fuel and cladding utilizing the generalized-plane-strain assumption for each axial segment and incorporating a large strain capability. The solution procedure, shown in Figure 5.1, involves iteration on local total strain within each time step, and it is explicit in time. Figure 5.2 shows the axial nodes (up to nine equal axial nodes over the fuel region and one node over the plenum region). Separate thermal and mechanical analysis segments/rings are considered by the code. Within the fuel region, each thermal ring can contain multiple mechanical rings. The fuel-cladding gap is represented by a single ring, and the cladding is represented by multiple thermal and mechanical rings. An additional ring can be present to represent the chemical interaction between the fuel and cladding as shown in the figure by the wastage range.

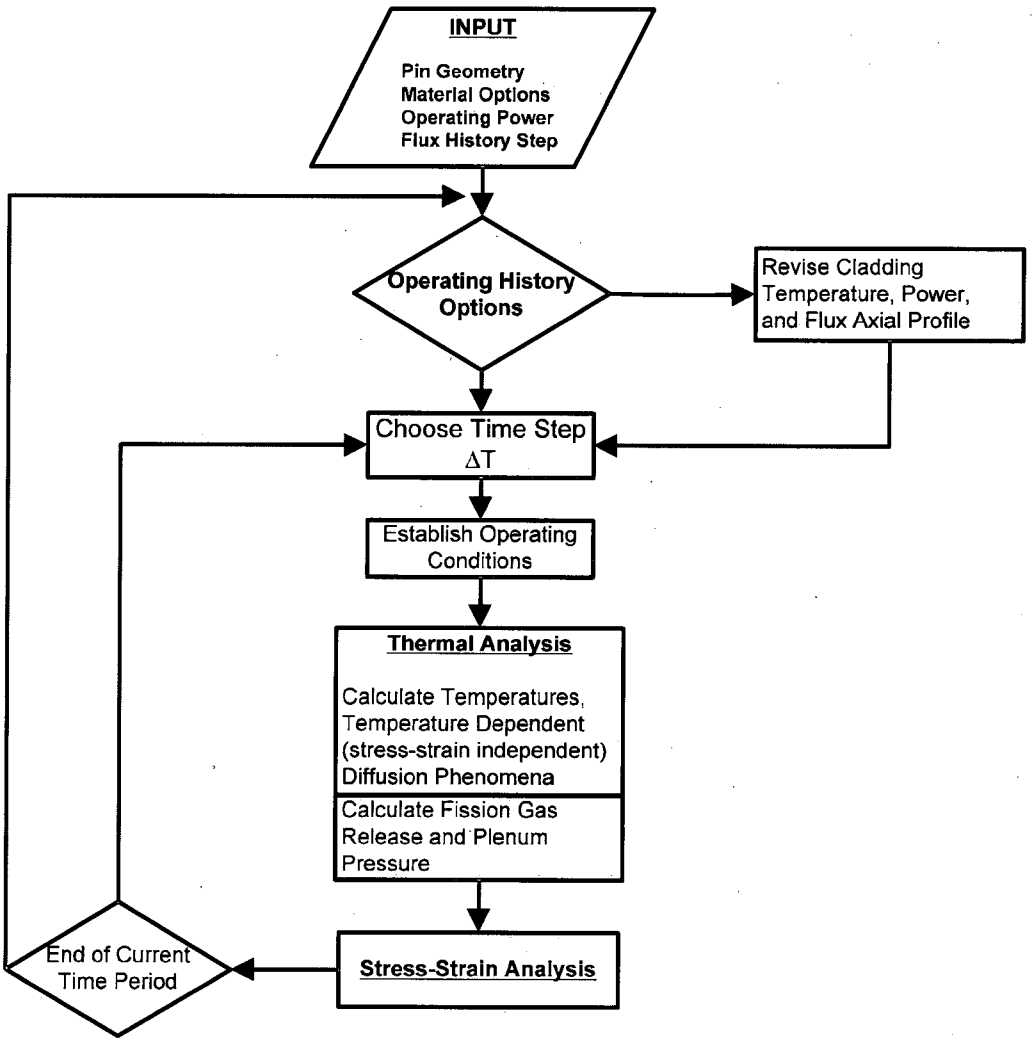

Figure 5.1. LIFE Code Solution Procedure

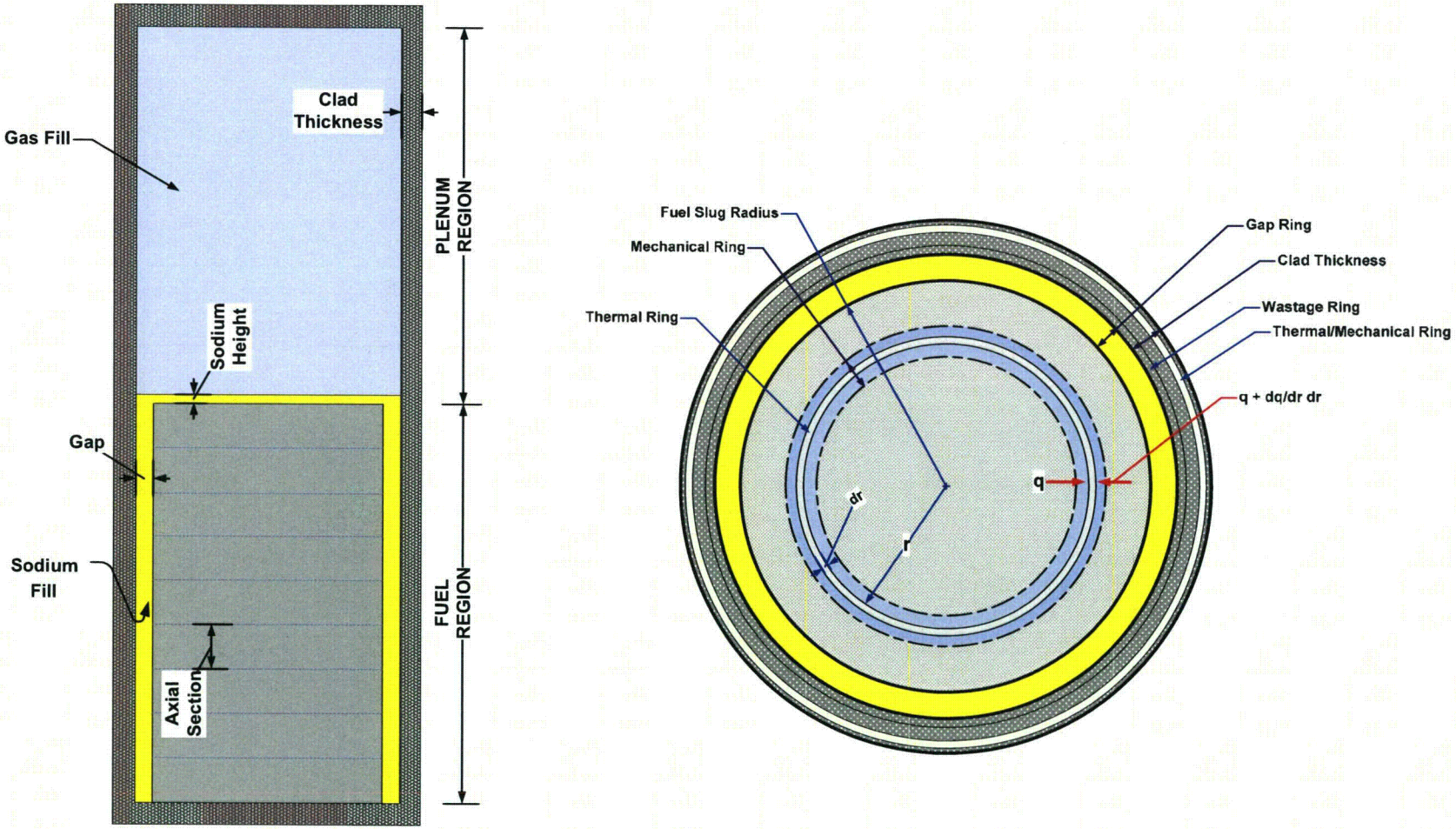

Figure 5.2. Fuel Pin Axial and Radial Representation in the LIFE Code

The system of equations (field equations) that are solved by the code are as follows:

- **Equilibrium**

$$r\frac{\partial \sigma_r}{\partial r} + \sigma_r - \sigma_\theta = 0$$

- **Kinematics**

$$\varepsilon_r^T = \frac{\partial u}{\partial r}, \varepsilon_\theta^T = u/r, \varepsilon_z^T = const.$$

- **Constitutive Relations**

$$\varepsilon_r^T = \frac{1}{E}\left[\sigma_r - \nu(\sigma_\theta + \sigma_z)\right] + \alpha T + \varepsilon_r^c + \varepsilon_r^s$$

$$\varepsilon_\theta^T = \frac{1}{E}\left[\sigma_\theta - \nu(\sigma_r + \sigma_z)\right] + \alpha T + \varepsilon_\theta^c + \varepsilon_\theta^s$$

$$\varepsilon_z^T = \frac{1}{E}\left[\sigma_z - \nu(\sigma_\theta + \sigma_r)\right] + \alpha T + \varepsilon_z^c + \varepsilon_z^s$$

- **Prandtl-Reuss Flow Rule**

$$\Delta\varepsilon_r^c = \frac{\Delta\varepsilon^c}{\bar{\sigma}}\left(\sigma_r - \frac{\sigma_\theta + \sigma_z}{2}\right),$$

$$\Delta\varepsilon_\theta^c = \frac{\Delta\varepsilon^c}{\bar{\sigma}}\left(\sigma_r - \frac{\sigma_\theta + \sigma_z}{2}\right),$$

$$\Delta\varepsilon_z^c = \frac{\Delta\varepsilon^c}{\bar{\sigma}}\left(\sigma_r - \frac{\sigma_\theta + \sigma_z}{2}\right),$$

where,

ε^T = *total strain*

u = *radial displacement*

ε^c = *creep strain*

ε^s = *swelling strain*

α = *thermal expansion coeff.*

$\Delta\varepsilon^c$ = *change in* ε^c *in time step*

$\bar{\sigma}$ = *equivalent stress*

In converting LIFE-4CN to LIFE-METAL, a number of fuel properties and models were changed and/or added. Fuel property correlations for U-5Fs and U-xPu-yZr were first developed as continuous functions of temperature, porosity, alloy composition, stress, fission rate, burnup, etc. The physical and thermal properties include density, phase-change temperatures, specific heat, thermal expansion, thermal conductivity, and alloy and fission product distributions. The mechanical properties include elastic moduli, fracture strength, and thermal- and fission-enhanced creep.

Physical, thermal, mechanical, and irradiation property correlations for the test and design cladding materials (e.g., austenitic 316, austenitic D9, and ferritic HT9) are included in the code. Some work has been done during LIFE-METAL development in improving the correlations (e.g., D9 creep and swelling) to get a better fit to the database within the operating range of interest for metallic fuels. The wastage correlation for sodium/cladding interaction and time and strain-failure correlations are also included. Models were developed for Ni depletion from D9 and carbon depletion from HT9 due to the fuel/sodium/cladding chemical interaction (FCCI). Empirical eutectic penetration correlations, based upon Fuel Behavior Test Apparatus (FBTA) and Whole-Pin-Furnace (WPF) test data [5.4, 5.5] are also incorporated in LIFE-METAL.

The focus of LIFE-METAL development has been on verifying the algorithms and validating the models for predicting fuel-pin behavior important in design analysis under normal operating conditions. Predictions of interest in the nuclear design are fuel length changes and changes in fissile content due to burnup and transmutation. Thermal predictions of interest are fuel temperature, design margins to fuel melting, and design margins to low-melting-temperature alloy (e.g., U-Fe) formation. Mechanical predictions of interest to designers are cladding damage and design margin to cladding failure due to fission gas pressure loading, fuel-cladding mechanical interaction (FCMI) and FCCI, and cladding deformation and design margin to significant coolant flow area reduction.

5.2 MODELS OF KEY PHENOMENA

As mentioned before, important metallic fuel (U-Zr and U-Pu-Zr) phenomena encountered in previous U.S. designs are related to FCCI, fuel constituent redistribution and swelling, and fission gas release [5.6]. These phenomena impact the degradation of cladding and the fuel swelling rates during operations. The following subsections discuss the treatment of the phenomena in the LIFE-METAL code. These models represent the main additions to the original oxide version of the LIFE code besides the other differences (fuel properties, gap conductance, elimination of oxide-related models, etc.).

5.2.1 Constituent Redistribution

This phenomenon is discussed in detail in Section 4.2. There are a number of performance-degrading issues associated with this phenomenon. The reduction of Zr fraction in areas within the fuel reduces the fuel melting points within those regions and potentially reduces the power to melt during accident sequences. During normal

operations, the temperature drop across the metallic fuel is low (usually < 250°C), as a result of the metal fuel high thermal conductivity, and the temperature drop across the fuel-cladding gap is negligible due to the presence of the sodium bond. This leads to a peak fuel temperature that is dictated by the limit on inner clad temperature, which is dependent on the type of cladding. For example, HT9 ferritic-martensitic steel has limited thermal creep properties that impose a nominal inner clad temperature of less than 620°C. This leads to peak fuel temperatures that are far from the melting temperature even in regions where the Zr is depleted.

A more significant effect of redistribution is its impact on the fuel swelling rates and axial fuel growth. The multiphase regimes present across the fuel radius, due to the redistribution phenomenon, with different growth rates, are believed to play a part in observed metal fuel anisotropic growth [5.7]. Anisotropic fuel growth, in which axial growth rate is lower than radial growth rate, was observed in fuel with higher Pu content as shown in Figure 4.3, and where constituent redistribution takes place. Reference 5.8 illustrates the possible impact of redistribution on fuel axial growth and fuel-cladding lock-up effects.

The axial fuel growth in the original LIFE code is treated through the isotropic growth of the fuel during irradiation. LIFE-METAL added the effects of anisotropic growth as follows. The axial swelling behavior is expected to cause swelling over the initial 1-1.5 at.% burnup, which produces the core dilution effect. Beyond that burnup, the fuel has contacted the cladding and additional axial growth is much slower. The initial axial growth is described by the following equations:

$$\Delta L/L_O\ (\%) = m_1 \times Bu \text{ for } Bu <= 0.75 \text{ at.\%, and}$$

$$\Delta L/L_O\ (\%) = 2.75 + m2 \times (Bu - 0.75) \text{ for } Bu > 0.75 \text{ at.\%}$$

where m_1 and m_2 are calibration constants, and in each case Bu is the peak fuel burnup (at.%). Note that the existing database for axial fuel growth shows considerable scatter, which can largely be explained by the fuel operating temperature. Outer row pins, which are colder, swelled more than inner row pins for the experiments.

Figure 5.3 shows an example of the LIFE-METAL predictions for fuel axial expansion versus data for U-10Zr fuel. Similar data are available for the ternary U-Pu-Zr fuel axial expansion.

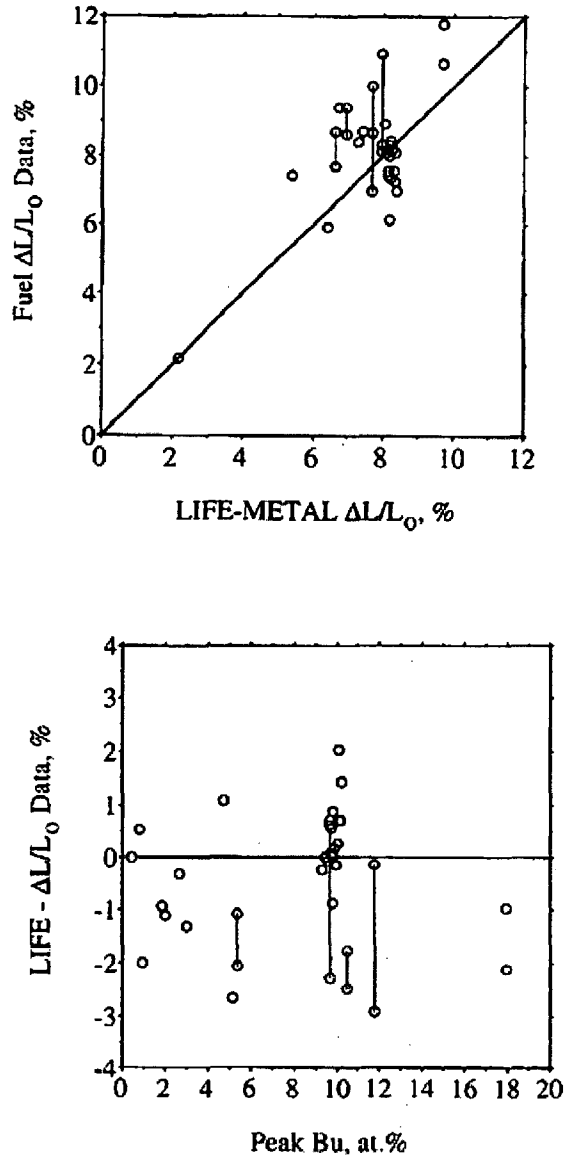

Figure 5.3. Predictions vs. Axial Expansion (ΔL/Lo) Data for U-10Zr Fuel

Computer models, not included in LIFE-METAL, were developed to calculate the redistribution of constituents in U-Zr and U-Pu-Zr metallic fuel under irradiation [5.9, 5.10]. The effective interdiffusion coefficients were parametrically determined using out-of-pile data to obtain a fit to the measured data as shown in Figure 5.4. This model can be a basis for further investigation using advanced simulation tools and atomistic level models to predict some of the model parameters and improve our understanding of the phenomena.

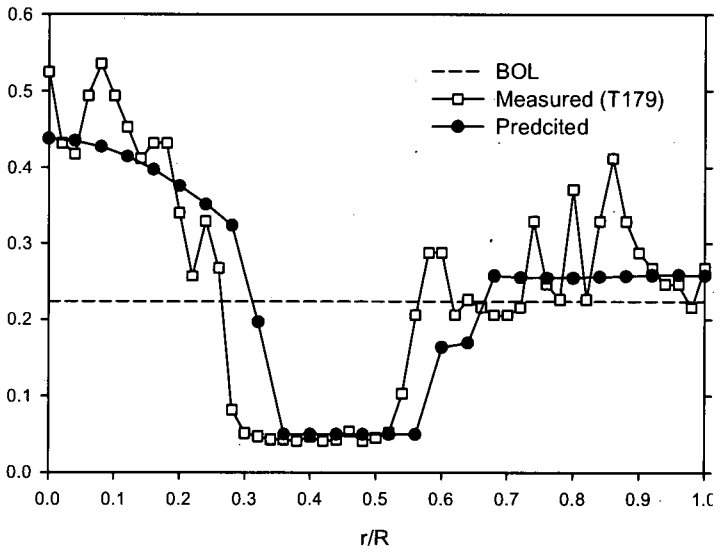

Figure 5.4. Comparison of Zr Redistribution Profiles of T179 by Prediction and by Measurement (Ref. 5.10)

5.2.2 Fuel Cladding Chemical Interaction (FCCI)

FCCI, discussed in Section 4.3 and shown in Figure 4.7, in which interdiffusion between the fuel and cladding components occurs, represents a two-fold potential problem for metallic fuel. It both weakens the cladding mechanical properties and leads to the formation of relatively low melting point compositions in the fuel. During normal operations, FCCI is characterized by solid-state interdiffusion, although liquid phase formation may occur during transients reaching 700°-800°C.

Attempts to model FCCI with empirical diffusion-type models were implemented in the LIFE-METAL code using collected cladding wastage data from fuel irradiated at EBR-II as shown in Figure 5.5 [5.11]. The figure shows an example of the results of code's estimates of the wastage data.

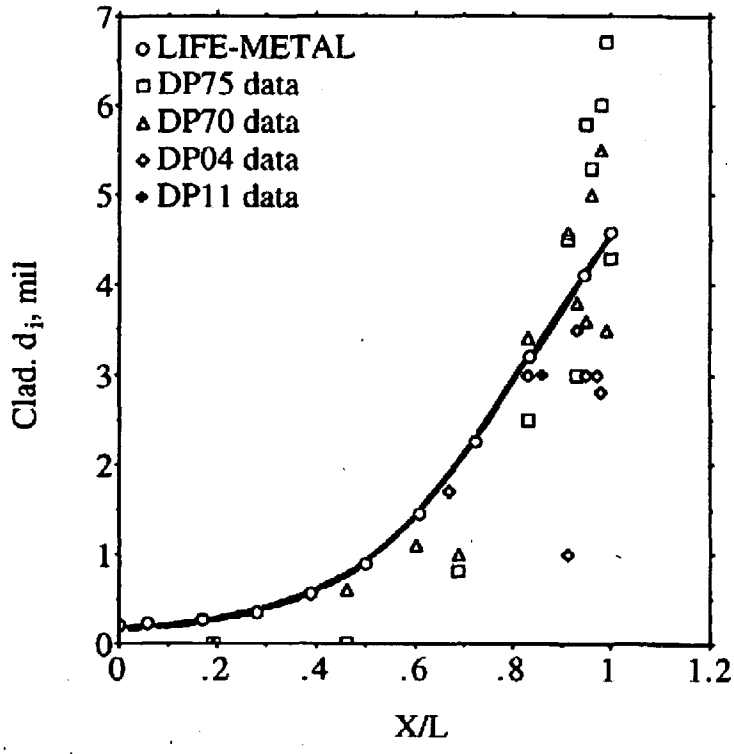

Figure 5.5. Predicted vs. Measured Axial Profiles of Fission Product Depth (D_i) in HT9 Stainless Steel Cladding for U-10Zr Elements DP04, DP11, DP70, and DP75 at 10 at.% Peak Burnup and PICT = 650° ± 10°C

LIFE-METAL has provisions to take wastage into account as follows. The cladding thickness is reduced from its nominal value due to 1) inner-diameter (ID) and outer-diameter (OD) fabrication tolerances and scratches; 2) OD sodium/cladding corrosion, decarbonization, and intergranular attack; and 3) ID fuel/cladding chemical or metallurgical interaction (FCCI). For both HT9 and 316SS claddings, ID FCCI is characterized by fission product (FP) diffusion into the cladding and some cladding constituent (e.g., Fe, Ni, Cr, C, etc.) diffusion from the cladding to the fuel. The fission-product-rich cladding layer tends to be very brittle (high microhardness) and susceptible to cracking. Thus, it cannot be relied upon as a load-bearing cladding layer. Let δo and δi be the cladding thicknesses (in mils) to be removed from the cladding OD and ID, respectively, for the structural analysis. In the LIFE-METAL approach, δo is removed from the cladding OD for both the thermal and mechanical analysis. This is reasonable in that it is assumed that the dominant contribution to δo is corrosion. In the case of ID corrosion, δi defines a cladding thickness layer that is present for both the thermal analysis and for determining fuel/cladding gap closure. However, the shear modulus is reduced by a factor of 10 and the creep rate of this layer is increased by a factor of 100 to make this fission-product-rich layer essentially non-load-bearing. It simply transmits the gas pressure or fuel/cladding mechanical interaction (FCMI) interface stress unabated to the intact base cladding.

It is recommended that a tolerance/scratch allowance of 0.5 mil be used for both the cladding ID and OD. Also, given the fact that temperature and operating conditions change with time, it is recommended that δo and δi be determined from rate laws:

$$\delta_o = 0.5 + \int_o^t \dot{\delta_o}\, dt, \text{ mils}$$

and

$$\delta_i = 0.5 + \int_o^t \dot{\delta_i}\, dt, \text{ mils}$$

The $\dot{\delta_o}$ functional form and parameters are determined from the cladding properties.

These rate correlations for clad ID corrosion are based on steady-state irradiation results and post-irradiation Fuel Behavior Test Apparatus (FBTA) and Whole-Pin-Furnace (WPF) test results. The HT9/U-xPu-10Zr database is used as a guide in modeling the HT9 in addition to the high-temperature HT9/U-10Zr database. For temperatures ≤ 650°C, the correlations for $\dot{\delta_i}$ are assumed to be of the diffusional form:

$$\dot{\delta_i} = 0.5 [D_o \exp (-Q/RT_{ci}) + D_{io} \phi]^{0.5} t^{-0.5}$$

where φ = neutron fast flux 10^{15} n/cm^2·s, R = 1.987 x 10^{-3} kcal/mol-K, T_{ci} = cladding ID temperature in K, D_O and D_{IO} are empirical parameters, and $\dot{\delta_i}$ = wastage rate in mils/h.

5.2.3 Swelling and Fission Gas Release

Swelling behavior of metallic fuel alloys is well documented [5.7]. As mentioned in Section 4.1, the general swelling behavior of those alloys is illustrated in Figure 4.4 by an increase in fuel length versus burnup. As shown in the figure, swelling proceeds rather rapidly with burnup, which is a characteristic of metallic fuel. Virtually all length increase takes place during that burnup interval before the swelling fuel pin contacts the cladding, < 1 at.% burnup. The leveling-off in axial swelling is thus determined by the fuel smeared density. As mentioned before, the behavior shown in the figure is an anisotropic behavior in which the axial growth proceeds more slowly than the radial growth, and the extent of anisotropy increases with increasing fuel Pu content. In the case of the 4S fuel, this anisotropy is expected to be limited due the lack of Pu in the fuel in addition to the fuel operating conditions, which inhibit the redistribution of the fuel constituents, thereby limiting the anisotropic growth. Currently, this axial growth behavior is represented in the LIFE-METAL code with a correlation and no mechanistic model is available. As mentioned before, a model that combines the predictions of constituent redistribution with axial lock-up effects was used to predict metallic fuel axial

growth [5.8]; however, the model has yet to be implemented in the LIFE-METAL code. This model uses fixed axial growth rates that are dependent on burnup, representing the two distinct axial growth regimes shown in Figure 4.4.

As for fission gas release modeling, although fission gas release models are available [5.12], they have not been implemented in the LIFE-METAL code. Again, fission gas release fractions are represented in the code by a correlation rather than a model. The fission-gas release model currently implemented in the LIFE-METAL code is summarized as follows. The model follows the gas release model implemented in the mixed-carbide and mixed-nitride version of the code, LIFE-4CN [5.1]. The parameters in the semi-empirical fission-gas-release and fuel-swelling models were changed to reflect the behavior of the uranium-alloy fuels of interest. These models have been described for carbide/nitride fuels and are reviewed briefly below to indicate what changes were made based on irradiation data for U-5Fs and U-xPu-Zr fuels. The rate of increase of retained fission gas in a fuel ring, $\dot{G}_s$, is found by a simple balance between the rate of gas production, $\dot{G}_p$ and the rate of gas release, $\dot{G}_r = F_g G_s$.

$$\dot{G}_s = \dot{G}_p - F_g G_s$$

The fractional release rate F_g is dependent on burnup (Bu in at.%), porosity (P), temperature (T), and fuel swelling strain (ε_s) due to gas bubbles according to:

$$F_g = \left[1 - e^{-\alpha \cdot Bu}\right] \cdot \left[1 + c_g \cdot (P - 0.1)^{-\frac{2}{3}}\right] \cdot R_g \cdot e^{\left(\frac{-Q_g}{R \cdot T}\right)} + f \cdot (\varepsilon_s - \varepsilon_{si}), \text{ in } \frac{1}{s}$$

where $(P - 0.1) \geq 0$, $(\varepsilon_s - \varepsilon_{si}) \geq 0$, and α, c_g, R_g, Q_g, f, and ε_{si} are empirical parameters to be determined from in-reactor data. For $\varepsilon_{si} \geq 0.3$, the second term is orders of magnitude larger than the first term in the equation for F_g, giving rapid gas release for fuel regions with gas bubble swelling >30%.

The LIFE-METAL fuel-swelling model includes the effects of incompressible and compressible fission-product swelling. The compressible (i.e., due to gas bubbles) fission-product-swelling strain is calculated from a model that assumes a number density c_b of bubble nucleation sites, which is independent of burnup but dependent on temperature according to:

$$c_b = B_b \cdot e^{\left(\frac{Q_b}{R \cdot T}\right)}, \text{ in } \frac{1}{cm^3},$$

where B_b and Q_b are empirical constants. The model also includes a non-equilibrium effect by allowing bubbles to grow to their equilibrium value at a rate proportional to the creep rate. Thus, more bubble nucleation sites are predicted to exist at lower temperatures, and the fewer gas atoms per bubble (along with the reduced rate toward equilibrium) will result in smaller bubbles and less swelling strain.

Figure 5.6 shows the predictions of LIFE-METAL versus U-10Zr fission gas release data. Similar data are available for fission gas release of U-Pu-Zr fuel.

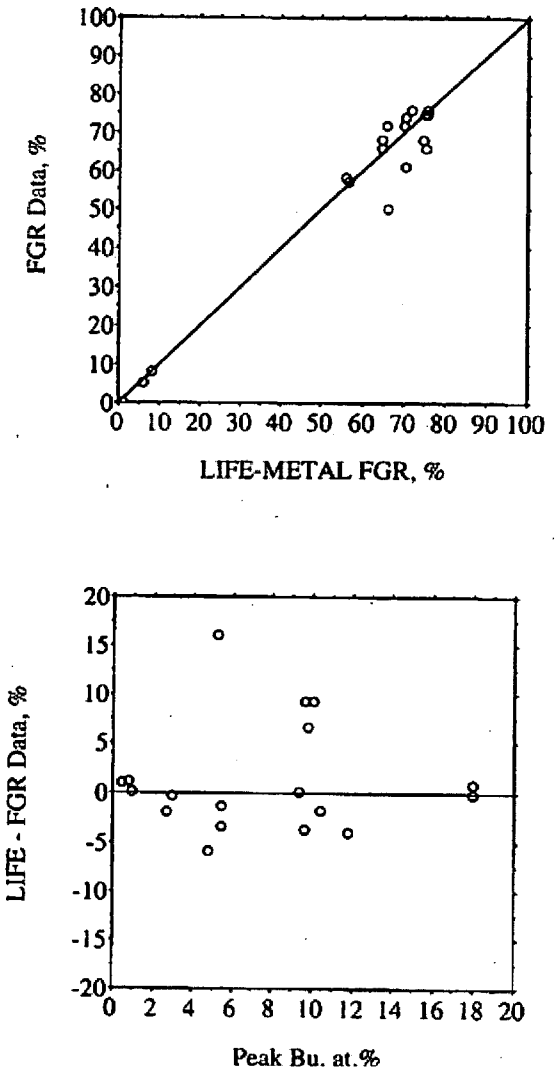

Figure 5.6. Predictions vs. Fission Gas Release (FGR) Data for U-10Zr Fuel

5.3 LIFE-METAL VALIDATION

The code validation effort has been extensive. Post-irradiation data are available from a large number of fuel-pin irradiations for "global" integrated parameters such as fission gas release, fuel volumetric change, and fuel length change. Axial profiles are available for fuel radial growth at low burnup (prior to and including initial fuel-cladding contact) and for cladding radial growth for a wide range of burnups and fast fluences. Other data available on a more limited basis are radial and axial variations in U, Pu, Zr, and fission gas porosity, axial variations in fraction of porosity filled (logged) with Na, and depth of C-depleted and Ni-depleted zones in HT9 and D9, respectively. Fairly complete sets of data are currently available for 80 fuel-pin irradiations (111 pins in total were used in the validation). Limited data (e.g., fuel length change, cladding diameter change) are available for hundreds of irradiated pins.

The validation database includes the data from 111 fuel element irradiations. This database includes the three cladding types (cold-worked, austenitic D9 and 316 stainless steels and HT9 ferritic/martensitic steel) and eight fuel compositions (U-10Zr, U-3Pu-10Zr, U-8Pu-10Zr, U-19Pu-6Zr, U-19Pu-10Zr, U-19Pu-14Zr, U-22Pu-10Zr, and U-26Pu-10Zr, where the numbers represent weight percents). The data from the 111 irradiations fall into one or more of the following categories: fission gas release (FGR), fuel axial strain ($\Delta L/Lo$), fuel diametral stain ($\Delta D/Dof$), cladding diametral strain ($\Delta D/Do$), and penetration depth (di) at the cladding inner diameter (ID) due to ingress of fission products (FP) and egress of cladding constituents. For the last three categories, axial profiles are often available. This implies a large number of data points per fuel element irradiation. Also, in the case of fuel axial expansion and peak cladding strain, which were routinely measured for all elements within a subassembly, the number of data points is much larger than the number of validation cases. When such data are available, the comparison is made between the LIFE-METAL prediction and the mean of the data with the $\pm$ one-sigma indicated. Table 5.1 summarizes the number of fuel/cladding combinations for the validation data set, as well as the number of data points for each category. The "+" superscript next to a number indicates that more data are available from sibling elements within a subassembly than used directly in the validation effort.

Table 5.1. Summary of Fabrication, Operating Conditions, and PIE Data for LIFE-METAL Validation (PICT is peak inner cladding temperature, FGR is fission gas release, $(\Delta L/L_O)_f$ is fuel axial strain, and $(\Delta D/D_O)_c$ is cladding diametral strain.)

				Number of PIE Data Points				
Fuel Type	Cladding Type	Burnup Range, at.%	PICT °C	FGR	Wastage	$(\Delta L/L_o)$	$(\Delta D/D_o)$ Peak	$(\Delta D/D_o)$ Profile
U-10Zr	D9 316SS HT9	0.8 - 18.0 0.5 - 5.0 2.8 - 18.5	535 620 500 530 660	10 3 4	14 - 30	13+ 4+ 19+	6+ 1+ 19+	5+ 0+ 7+
U-3Pu-10Zr	316SS	0.5 - 5.0	500	4	-	4+	1+	0+
U-8Pu-10Zr	D9 316SS HT9	0.8 - 18.0 0.5 - 5.0 2.8 - 16.0	535 565 500 530	10 4 1	- - -	11+ 4+ 3+	5+ 0+ 1+	5+ 0+ 1+
U-19Pu-10Zr	D9 316SS HT9	0.8 - 18.0 0.5 - 5.0 2.8 - 19.5	535 590 500 530 590	12 4 8	21 6 9	14+ 4+ 9+	9+ 2+ 17+	9+ 0+ 10+
U-19Pu-6 Zr	HT9	5.0 - 10.0	575	2	-	1+	2+	1+
U-19Pu-14Zr	HT9	6.0 - 13.0	590	2	-	2+	2+	1+
U-22Pu-10Zr	316SS	0.5 - 5.0	500	4	-	4+	1+	0+
U-26Pu-10Zr	316SS HT9	0.5 - 5.0 2.2	500 534	3 1	- -	4+ 0+	1+ -	0+ -
DATA TOTAL				72	80	92+	68+	51+

An example of a validation data set is the HT9 data set from EBR-II subassembly X441. This data set has a peak cladding temperature of 600 °C and peak linear heat rating of 16 kW/ft (52.5 kW/m). The reference X441 pin cladding thickness is 15 mils (0.038 cm), and the typical EBR-II fuel and cladding dimensions. The design variables included in X441 are Zr content (6-14 wt.%), plenum-to-fuel volume ratio (1.0-2.1), and fuel smeared density (70-85%). Code predictions were compared to experimental data for cladding strain, fuel length change, and fission gas release. Figure 5.7 shows the good agreement between the LIFE-METAL predictions and the data for the peak HT9 cladding strains (circles) for 75% smeared density U-19Pu-10Zr pins. The difference between LIFE predictions and data is generally within the uncertainty and pin-to-pin scatter (~0.087%). Also included in Figure 5.7 are some data from subassembly X425 at lower power, cladding temperature, and plenum-to-fuel volume ratio. Each point in the figure represents approximately four pins.

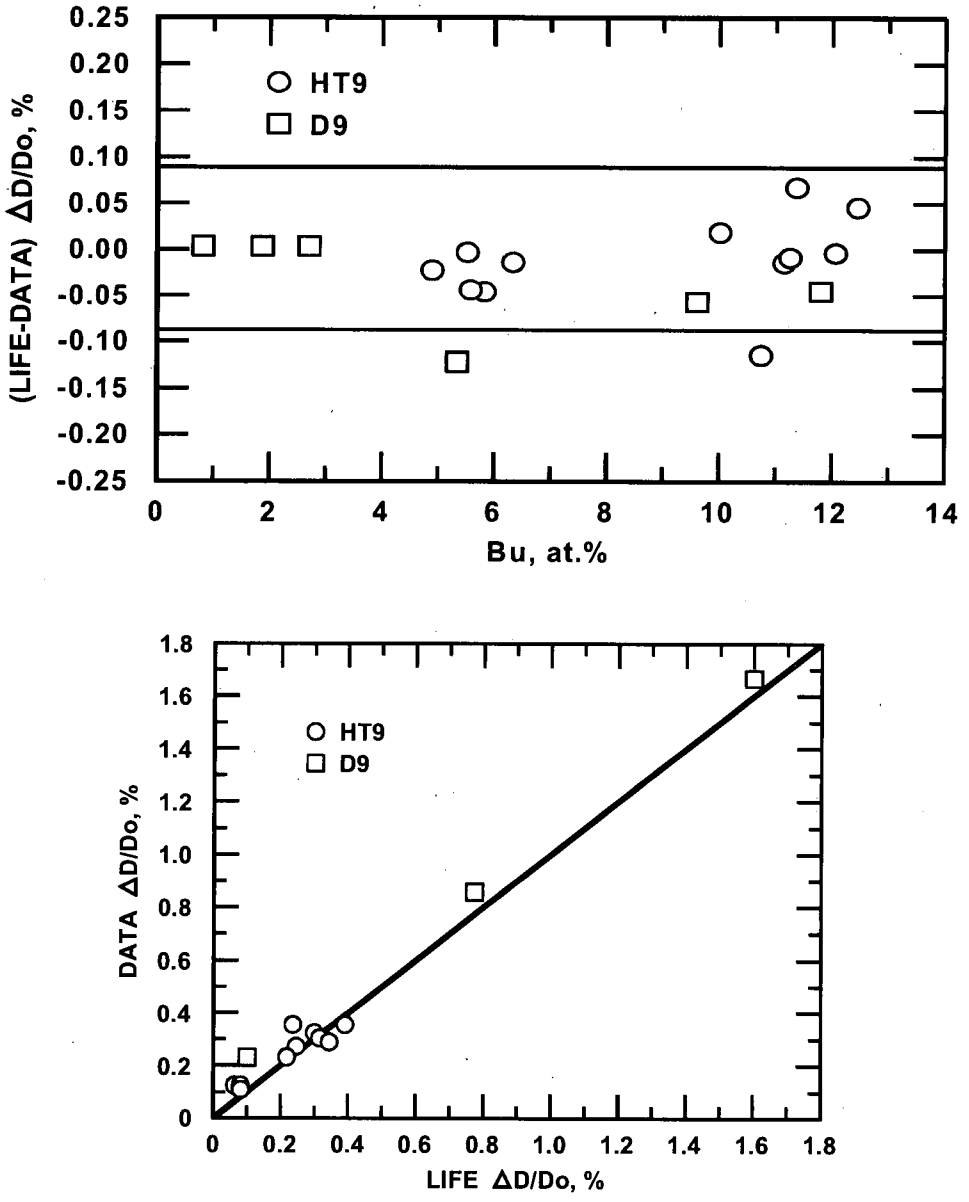

Figure 5.7. LIFE-METAL vs. Data for U-19Pu-10Zr/HT9

In addition to Figure 5.7, Figures 5.3, 5.5, and 5.6 also show other validation results. Those results include axial growth, fission products depth of penetration, and fission gas release in Figures 5.3, 5.5, and 5.6, respectively.

5.4 APPLICABILITY OF LIFE-METAL FOR EVALUATING THE 4S LONG-LIFE METALLIC FUEL

As shown in Table 2.2, the 4S fuel design has both dimensional and operational differences from the typical fuel designs of EBR-II and FFTF, which constitute the irradiation database and the database used in the validation of the LIFE-METAL code. However, those differences do not appear to have a significant impact on the code's estimates as indicated next.

The fuel length of 2.5 meters compared to the typical length of about 0.3 (EBR-II) to 0.9 meter (FFTF) does not affect the LIFE-METAL calculations, since the code ignores axial heat conduction and there are no provisions for mechanical coupling between axial nodes. The only connection between the axial nodes is thermally as the axial nodes are coupled through the calculated coolant temperatures. Doubling the diameter of the fuel slug and the cladding thickness has no impact on the fundamental code assumption related to estimation of stresses on the cladding, i.e., that the cladding is a thin-walled vessel. This assumption holds as long as the cladding wall thickness remains much less than the inner cladding radius, which is the case for the 4S fuel, since doubling the cladding thickness is compensated for by also doubling the fuel radius relative to the earlier fuel. For example, the hoop stresses due to the plenum gas pressure is proportional to the ratio of the cladding thickness to the cladding inner radius. Another dimensional difference between 4S fuel and typical fuel is the slightly higher smeared density of 78% compared to 75%, which has no impact on the code calculations, since the 78% density lies within the experimental database. Also, it lies within the range of optimal density between 75% and 80%, which leaves room for enough fuel swelling before contact with the cladding that allows the release of significant amounts of fission gasses to the plenum. The ratio of the plenum to fuel volume is within the range of the ratios associated with the LIFE-METAL validation database.

The operational differences include the much smaller burnup and linear power of the 4S design, and the corresponding lower fuel temperature and fuel temperature drop across the fuel cross-section. Lower fuel temperature and temperature drop have no impact on the validity of the code's calculations. Thermal expansion of the fuel and the cladding represents only a small fraction of the dimensional changes that the fuel undergoes during irradiation and the fuel temperature remains within the lower range of temperatures for which the code was validated. The FCCI depends mainly on the temperature at the fuel-cladding interface and fuel burnup, which are both within the validation range of the code, though at the lower end of the database range. Although the fission gas release correlation used in the code depends on fuel temperature, this dependence is much weaker than the dependence on burnup. The fast fluence exposure and peak cladding temperature of the 4S fuel are within the ranges of the experimental data (again, the lower range). The extended life of the 4S, that is, operation to 30 years, does not affect the validity of the code, since there are no specific assumptions in the code models regarding the operational time. The peak fast fluence, which is dependent on time, remains less than the peak exposure of HT9 cladding. The HT9 thermal creep

correlation is also time dependent. Although the experimental database for this correlation is much less than the lifetime of the fuel, it is believed that the correlations are still valid for the 30 years of operation given the very low stresses from fission gas loading in the case of the 4S fuel. Improved long-time correlations are the subject of current interest [5.13, 5.14]. Finally, the linear power for the 4S fuel is much lower than that for the pins used in the LIFE-METAL validation. However, the burnup rather than the linear power is the driving force for the code's phenomena correlations such as fission gas release, axial growth, and FCCI. Thus, there is no direct dependence on linear power other than the determination of the fuel temperature and temperature drop.

REFERENCES 5

5.1 M. C. Billone, Y. Y. Liu, E. E. Gruber, T. H. Hughes, and J. M. Kramer, "Status of Fuel Element Modeling Codes for Metallic Fuels," Proc. ANS International Conference on Reliable Fuels for Liquid Metal Reactors, September 7-11, 1986, p. 5-77.

5.2 V. Z. Jankus and R. W. Weeks, "LIFE-II – A Computer Analysis of Fast Reactor Fuel-Element Behavior as a Function of Reactor Operating History," *Nuc. Eng. and Des., 18* (1972) 83-96.

5.3 Y. Y. Liu; S. Zawadzki, M. C. Billone, U. P. Nayak, T Roth, "Development of LIFE4-CN: a combined code for steady-state and transient analyses of advanced LMFBR fuels," Post-SMiRT5 second international seminar on mathematical/mechanical modeling of reactor fuel elements; 20 Aug 1979; Berlin, F.R. Germany.

5.4 H. Tsai, "Fuel/Cladding Compatibility in Irradiated Metallic Fuel Pins at Elevated Temperatures," International Fast Reactor Safety Meeting, Snowbird, Utah, August 12-16, 1990.

5.5 J. M. Kramer, Y. Y. Liu, M. C. Billone, and H. C. Tsai, "Modeling the Behavior of Metallic Fast Reactor Fuels During Extended Transients," Journal of Nuclear Materials, 204, (1993), pp. 203-211.

5.6 A. M. Yacout, G. L. Hofman, J. D. B. Lambert, and Y. S. Kim, "Fuel Behavior Modeling Issues Associated with Future Fast Reactor Systems," GLOBAL 2007, Boise, Idaho, 2007.

5.7 G. L. Hofman and L. C. Walters, Chapter 1, "Metallic Fast Reactor Fuels," in "Material Science and Technology, A Comprehensive Treatment," Volume 10A, Edited by R. W. Cahn, P. Haasen, and E. J. Kramer, 1994.

5.8 Y. S. Kim, A. M. Yacout, G. L. Hofman, and Ho Jin Ryu, "U-Zr Constituent Redistribution, Gap Closure, and Axial Growth in Reduced-Power Fast Reactor Fuel Designs," ANS Meeting, Boston, MA, June 24-28, 2007.

5.9 G. L. Hofman, S. L. Hayes, M. C. Petri, "Temperature Gradient Driven Constituent Redistribution in U-Zr Alloys," Journal of Nuclear Materials, 227, (1996) 277-286.

5.10 Yeon Soo Kim, G.L Hofman, S. L. Hayes, and A.M. Yacout, "Modeling of Constituent Redistribution in U-Pu-Zr Metallic Fuel," Journal of Nuclear Materials, 359, (2006) 17-28.

5.11 M. C. Billone, Argonne National Laboratory, Private Communications, 1994.

5.12 J. Rest, "Kinetics of Fission-Gas-Bubble-Nucleated Void Swelling of the Alpha-Uranium Phase of Irradiated U-Zr and U-Pu-Zr Fuel," Journal of Nuclear Materials, 207, 192 (1993).

5.13 Ho Jin Ryu, A. M. Yacout, Yeon Soo Kim, G. L. Hofman, "Review of HT9 Cladding Creep Correlations for Advanced Liquid Metal Fast Reactors," ANS Embedded Topical Meeting: Nuclear Fuels and Structural Materials for the Next Generation of Nuclear Reactors, Reno, Nevada, June 4-8, 2006.

5.14 Ho Jin Ryu, Yeon Soo Kim, A. M. Yacout, "Thermal Creep Correlation of HT9 Ferritic Martensitic Steel for Liquid Metal-Cooled Fast Reactor Fuel Cladding," Submitted to Journal of Nuclear Materials.

6. FUEL DESIGN EVALUATION CRITERIA

This section is based on the design criteria that were developed for the EBR-II Mark-V metallic fuel pins in 1994 [6.1, 6.2] as part of the safety case for the introduction of this fuel into EBR-II. Those criteria are based on experience from PRISM and Clinch River Breeder Reactor (CRBR) criteria, combined with our general experience of the behavior of metallic fuel clad in HT9 steel under irradiation. The criteria presented herein establish the detailed criteria that the fuel pin design must satisfy in order to meet general requirements and establish the methodology that should be used. These criteria were selected so that the fuel pins will satisfy their functional requirements and performance objectives in a safe and reliable manner based on current technology. The functional requirements of the fuel design are discussed first, followed by the design criteria that are put in place to meet those functional requirements.

6.1 FUNCTIONAL REQUIREMENTS

The primary functions of the fuel subassemblies in a reactor are to provide, protect, and position the nuclear fuel to produce heat for the reactor heat transport system. Specific design features in the fuel subassemblies also serve important safety functions. The fuel pin cladding acts as the primary fission product barrier and the duct helps to protect the reactivity control system and the primary cooling system, both during normal operation and during off-normal events. The design requirements for the fuel ensure that these functions will be fulfilled. The two principal requirements that have been established to meet the safety and reliability functions for the 4S fuel subassemblies based on experience with EBR-II are:

1. Ensure that sufficient fuel pin reliability is maintained to statistically prevent a "significant" number of fuel pin breaches during normal and off-normal reactor operation including postulated accidents. A "significant" number of breaches may be defined as that which challenges the safe operation or performance goals of the reactor. This has previously been defined as ensuring that no more than one fuel pin breach is expected per core loading. Here, it is defined as ensuring that no more than one fuel breach is expected per one effective full-power year of operation.

The calculable performance guidelines, as shown subsequently in Table 6.1, have been formulated to ensure this reliability requirement. Factors involved in the assessment and guarantee of reliability are 1) prevention of stress rupture of the cladding, which involves fuel pin materials choices that ensure the peak cladding temperature is below the minimum fuel/cladding eutectic temperature for steady-state operation and a burnup limit at which point creep damage caused by fuel and fission-product-induced stress does not compromise cladding integrity (this is not a concern for the low burnup 4S fuel), and 2) a fuel design and fabrication specification that will statistically eliminate manufacturing defects sufficient to cause reduced reliability.

2. Maintain a coolable geometry of both the fuel pin and the fuel pin bundle for the useful lifetime of the subassembly, including normal operation and all off-normal events (Anticipated Operational Occurrences (AOOs) and postulated accidents).

The coolability requirement is demonstrated by analytical performance assessment (thermal-hydraulic safety analysis) and by the existing in-reactor experimental database. During normal operation, anticipated events and postulated accidents, the low probability of fuel pin failure ensures that the fuel pins will remain intact and, therefore, that the coolable pin bundle geometry will be maintained. In addition, established limits (see next section) on fuel melting, fuel/cladding eutectic formation, maximum cladding stress, and maximum cladding strain ensure no "significant" number of pin failures for these events.

6.2 DESIGN CRITERIA

The design criteria and analysis methods presented in this section address the geometry, temperature regimes, and loading mechanisms that are expected to influence fuel performance during normal operations. Certain loading conditions are not reflected by the criteria because they have been eliminated by proper design of the 4S fuel. For example, bundle-duct interaction (BDI), which could impose a limit on the total cladding strain, is not an issue with the low-swelling HT9 cladding and duct, and also given the low end-of-life (EOL) burnup and fluence of the fuel. Similarly, stress loading on the cladding from fuel-cladding mechanical interaction (FCMI) is also not an issue for this design, again because of the low fuel burnup. No design criteria were considered for either issue since they do not represent a life-limiting concern.

Although it may be desirable to have a single set of criteria for all conditions (steady state and transient), it is recognized that, because of the widely different time scales involved, separate criteria are necessary. Evaluations of steady-state operation are made using current, state-of-the-art metallic fuel behavior models as incorporated in the LIFE-METAL code [6.3], described in detail in the previous chapter. Evaluations of the transient behavior of the 4S fuel are performed as an integral part of the whole-core analyses of the response of the reactor to accident conditions, and are not included in this report. Thus, the design criteria given below are those that are applicable to normal operation of the fuel.

The reference cladding for the 4S fuel is the ferritic/martensitic HT9 steel alloy. Although the CRBR design was never built, a Preliminary Safety Analysis Report (PSAR) was written and the U.S. Nuclear Regulatory Commission (NRC) issued a memorandum of findings that would have resulted in the granting of a construction permit [6.4]. Similarly, PRISM design criteria were reviewed by the NRC [6.5] and its review of the fuel qualification plan was related to the U-Pu-Zr and U-Pu-MA-Zr fuel with no negative comments on the metal fuel performance in general. As mentioned before, criteria for those two designs as applied to the EBR-II Mk-V fuel safety case are the basis for the following criteria summarized in Table 6.1.

Table 6.1. Steady-State Design Criteria Considered for the 4S Fuel

	Design Criteria
1.0	$\varepsilon_{THN} \leq 1\%$
2.0	$CDF_N \leq 0.05$
3.0	No fuel melting
4.0	No eutectic liquefaction at the fuel-cladding interface
5.0	$\overline{\sigma}_H < 150\ MPa$

ε_{THN} = thermal component of plastic hoop strain during normal operation

CDF_N = cumulative damage function during normal operation

$\overline{\sigma}_H$ = radially averaged primary hoop stress

1.0 During steady-state (normal) operation, the thermal component of the plastic diametral strain for HT9 cladding shall be less than 1%.

The total in-reactor, permanent strain consists of a volumetric swelling strain and an in-reactor creep strain. The in-reactor ductility of a pressurized tube is often associated with the thermal creep strain component. For HT9 cladding, there is a small database for failure strain that corresponds to in- and out- of reactor pressurized tube tests [6.6]. The lowest observed failure strain in those tests was about 2.0%. Thus, a 1% limit is conservative. Also, based on the limited data, it appears that there is no significant difference in the time at pressure and temperature to cause failure, whether the test was performed in-reactor or out-of-reactor. This observation supports the concept that it is the thermal creep component that is damaging for HT9 cladding.

Very few HT9 breaches have occurred in irradiated metallic fuel pins in EBR-II. Two breaches, out of 15 pins exposed to the same conditions, occurred in HT9/U-10Zr pins from EBR-II Subassembly X447A at 10 at.% burnup [6.7]. These 15 pins were operated at a peak nominal beginning-of-life cladding temperature of 644° ± 12°C. The maximum diametral strain for unfailed sibling pins reached 2%, which is above the prescribed design limit for the current design.

2.0 During steady-state operation, the cumulative damage function (CDF) for HT9 cladding shall be limited to 0.05.

The CDF, or life fraction, is a widely used method for predicting failure of components that are subjected to creep damage at elevated temperatures and has been accepted as a means for predicting fuel pin failure in LMR systems [6.8]. The CDF method allows rupture time data from creep tests at constant stress and temperature to be used to predict failure under similar loading conditions, but with time-varying stress and temperature. The basic assumption is that creep damage is linearly additive so that the damage over a given time interval *dt* is proportional to the ratio of the time interval to the time t_r that would cause failure at the instantaneous stress and temperature levels. The CDF is then defined as the sum of these fractions, or

$$CDF = \int_0^t \frac{dt}{t_r}$$

The expected value of the CDF at failure should equal 1.0 in order to be consistent with the database for t_r. However, in practice, the allowable CDF is usually chosen to be smaller than 1.0 to account for differences in loading conditions from those assumed, uncertainties in the applied temperature and stress histories, and scatter in creep-rupture database.

The CRBR PSAR utilized the CDF as a design criterion to ensure that fast reactor cladding satisfies its functional requirements during the fuel lifetime. Here, the allowable CDF is separated into a steady-state component and a transient component, which departs somewhat from the format used in the CRBR PSAR. For CRBR, the equivalent requirement was that the sum of the steady-state CDF plus the accumulated CDF for all transients should be less than 1.0 [6.9]. Here, a CDF of 0.05 for steady-state operation has been allowed. The CDF for HT9 cladding is calculated using long-term stress-rupture correlations. The hoop stress used in this correlation is to be calculated from the plenum gas pressure and/or the fuel-cladding interface pressure using the same formula as was used to correlate the data.

The CDF methodology has been validated by comparing the results of variable-load and -temperature tests with predictions based on results of constant-load and -temperature tests along with the CDF law [6.10]. Less direct evidence of the validity of the CDF method for predicting HT9 cladding lifetime is its successful use in the analyses of the TREAT tests and the Whole-Pin-Furnace tests on HT9 clad metallic fuel pins. Notice here that the CDF failure criterion and the strain-to-failure criterion given above are not totally independent, so that satisfying both design requirements adds a degree of conservatism through redundancy. The relationship between the two criteria comes from the definition of the CDF along with the Monkman-Grant relationship [6.11], which empirically relates the secondary creep strain rate $\dot{\epsilon}$ to the rupture time t_r by

$$\dot{\epsilon}\, t_r = \text{constant}.$$

The allowable CDF of 0.05 during steady-state operation of the 4S fuel pins with HT9 cladding is based on the HT9 out-of-reactor stress-rupture data and LIFE-METAL code calculations for fuel pins with HT9 cladding that have been irradiated in EBR-II. With regard to the time-to-rupture correlation used in the CDF formulation, it is fit to the unirradiated stress-rupture data for pressurized HT9 tubes. A statistical analysis [6.12] of these data shows the logarithm (base 10) of the CDF at failure is distributed normally. With 95% confidence, the mean and standard deviation of the probability distribution are -0.0354 and 0.1885, respectively. Thus, the failure probability will be less than 1 in 3000 if the logarithm of the CDF is less than -0.6771, or the CDF is less than 0.21. The allowable value of the steady-state CDF of 0.05 that is used in the current safety case is considerably smaller than this value. The additional conservatism is based on the precedent set by CRBR and PRISM reactor analyses, engineering judgment, and the desire to select a suitably low value of the steady-state CDF so that it can be argued that the transient performance of the cladding is not significantly degraded by the steady-state operation.

It is worthwhile to also consider the database for irradiated HT9/U-Pu-Zr fuel pins. In terms of the calculated (using the LIFE-METAL Code) CDF values for HT9/U-19Pu-10Zr fuel pins that did not fail, most of the calculated values are in the range of 10^{-6} to 10^{-8} for peak burnups of 10-12 at.%. However, four fuel pins from subassembly X441, which had high smeared densities (85%), reached 10 at.% burnup without failure. The calculated CDF was 0.2 for these pins, which exhibited substantial fuel-cladding mechanical interaction.

3.0 During steady-state operation, the power in the hottest fuel pins, regardless of cladding type, shall be less than the minimum values for incipient bulk fuel melting. The redistribution of fuel alloying elements shall be considered in satisfying this criterion.

The purpose of the above requirement is to provide sufficient margin up to the overpower reactor trip points so that incipient fuel melting is precluded. This is not meant to imply that incipient fuel melting under these conditions is, in itself, detrimental. Rather, by providing such a margin, the task of demonstrating that reactor accident transients can be terminated with limited fuel damage becomes easier.

It has been traditional practice in license applications to the Nuclear Regulatory Commission to assume that failure of nuclear reactor fuel pins will occur if bulk (centerline) fuel melting takes place [6.13]. The origin of this assumption comes from light water reactor practice for uranium oxide fuels, for which the criterion was established to ensure that molten fuel could not come into contact with the cladding. Because the melting point of uranium dioxide (2700°C) is much greater than the melting point of the cladding (~1400°C for iron-based materials), contact of the cladding by molten oxide fuel can lead to melt-through or significant weakening of the cladding. The damage caused to the cladding depends on the mass of the molten fuel that reaches the cladding through cracks in the fuel pellets. This is obviously difficult to predict with any

degree of certainty. Consequently, it is easier for light water reactor fuel safety analyses to simply exclude fuel melting.

Bulk fuel melting is less likely to cause cladding damage in metallic fuel pins because the melting temperature of the fuel (~1100°C) is less than the melting temperature of the cladding. The relatively benign effect of bulk melting in metallic fuels is illustrated by the results from experimental irradiations of EBR-II Mark-IA fuel fabricated with bond sodium only in the lower half of the pins. Even though the absence of the bond caused extensive fuel melting, the molten fuel simply relocated to close the fuel-cladding gap and froze in place without failing the cladding. Only a small area of eutectic interaction with the cladding was noted with a maximum wall penetration of 10% of the thickness.

It should be noted here that the bulk fuel melting criterion is being applied to the fuel alloy itself (U-Zr) and not to the low-melting-point fission products or to alloys that these fission products may form with the fuel constituents. Just as it is impossible to preclude local melting in the vicinity of fission tracks, it is impossible to preclude small amounts of liquid formation caused by the fission products. This microscopic melting is not damaging to the fuel or to the cladding. In the case of the 4S fuel, this criterion overlaps with the following criterion of maintaining a fuel-clad interface temperature lower than the eutectic temperature, because the temperature gradient across the fuel is very low (<100°C), which implies that the fuel will not reach the melting temperature of about 1100°C as long as criterion *4.0* is met (the eutectic temperature is between 650° and 750°C, which implies peak fuel temperature of less than 1000°C).

4.0 Within the bounds of normal operation and reactor maneuvering, the power-to-flow ratio and power in the hottest fuel pins, regardless of cladding type, shall be less than the minimum values for macroscopic eutectic liquefaction at the fuel-cladding interface.

Exceeding the eutectic liquefaction temperature while within the bounds of normal operation is not acceptable to meet functional requirement (1), Section 6.1. The temperature threshold can be exceeded, however, for short times during off-normal reactor operation, outside the bounds of normal operation, without excessively damaging the fuel pins.

The source of the eutectic liquefaction at the interface is the metallurgical interaction of metallic U-Zr fuel and fission products with the iron-based cladding to form a low-melting-point phase. Just as it is impossible to preclude microscopic melting within the bulk of the fuel, it is equally impossible to preclude microscopic fuel melting at the interfaces between certain phases that may form at the fuel-cladding interface. However, the safety and reliability concerns involve ensuring that the cladding remains intact and that fuel motion cannot lead to increases in reactivity or regions of high smeared density. The above limits are designed to satisfy these concerns. For the 4S U-10Zr/HT9 fuel/cladding, the maximum interface temperature for which macroscopic

liquefaction does not occur is taken to be 650°C (the hot-spot peak cladding temperature is about 609°C).

5.0 During normal operation, the plenum pressure shall be less than that which would cause a peak, radially averaged hoop stress in the cladding of 150 MPa in the hottest pin.

The purpose of this limit is to preclude unstable plastic deformation. The parallel criterion in the CRBR PSAR was that the primary equivalent stress remain below 90% of the yield strength. However, the yield strength of cladding materials at high temperatures depends on the strain rate at which the defining tensile tests are performed. Thus, using the yield strength as a limit does not uniquely define the criterion unless the strain rate is specified. On the other hand, the flow stress for HT9 cladding material does become nearly strain-rate independent above a certain stress, which depends on the temperature. If the cladding is subjected to stresses near this level, the strain rates increase very rapidly. The primary loading due to internal gas pressure is most damaging in this regime because it can lead to plastic instability. Stresses caused by secondary loads, such as thermal stresses, do not lead to plastic instability since the plastic deformation acts to relieve the stresses. Since internal gas pressure is the only loading that leads to plastic instability, a limit on gas pressure, or, rather, on the radially averaged hoop stress caused by gas pressure, is the appropriate criterion for precluding plastic instability. Criterion 5.0 therefore includes only the hoop stress produced by gas pressure, not stress from fuel-cladding mechanical interaction (FCMI), since stress from FCMI does not lead to plastic instability.

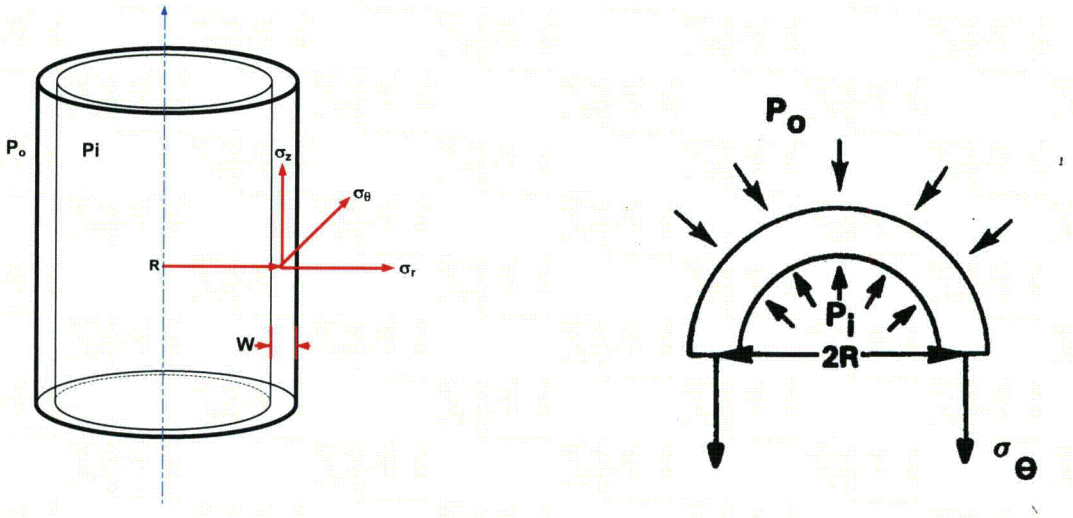

Figure 6.1. Stresses on Thin-Walled Tube

The value of 150 MPa for the hoop stress limit was set by limiting the gas pressure, or hoop stress, to levels below which burst failures do not occur in pressurized cladding tubes. It is argued that plastic instability would not occur if the cladding hoop stress remained below the high-stress branch of the biaxial stress rupture curves. The locus of points that define the intersection of the high-stress and low-stress branches of these curves is a weak function of temperature for HT9 cladding materials. The high-stress branches always begin at hoop stresses greater than 150 MPa for temperatures below 650°C.

REFERENCES 6

6.1 L. Briggs, et al., private communications, March 1995.

6.2 L.K. Chang, D. J. Hill, and J. Y. Ku, "A Method for the Determination of Technical Specifications Limiting Temperatures in EBR-II Operation," Fourth International Topical Meeting on Nuclear Thermal Hydraulics Operation and Safety, April 5-8, 1994, Taipei, Taiwan, R.O.C.

6.3 M. C. Billone, Y. Y. Liu, E. E. Gruber, T. H. Hughes, and J. M. Kramer, "Status of Fuel Element Modeling Codes for Metallic Fuels," Proc. ANS International Conference on Reliable Fuels for Liquid Metal Reactors, September 7-11, 1986, p. 5-77.

6.4 U.S. Nuclear Regulatory Commission, "Safety Evaluation Report Related to the Construction of the Clinch River Breeder Reactor Plant," NUREG-0968, Volume 1, March 1983.

6.5 "Preapplication Safety Evaluation Report for the Power Reactor Innovative Small Module (PRISM) Liquid-Metal Reactor," NUREG-1368.

6.6 A. E. Bridges, A. E. Waltar, R. D. Leggett, and R. B. Baker, "A Liquid-Metal Reactor Core Demonstration Experiment Using HT9," Nuclear Technology, 102, (1993) pp. 353-366.

6.7 R. G. Pahl, C. E. Lahm and S. L. Hayes, "Performance of HT9 Clad Metallic Fuel at High Temperature," J. Nucl. Mater., 204, (1993) 141-147.

6.8 Alan E. Waltar and Albert B. Reynolds, "Fast Breeder Reactors," Pergamon Press, 1981.

6.9 Y. S. Tand, R. D. Coffield, R. A. Markely, "Thermal Analysis of Liquid Metal Fast Breeder Reactors," Publisher American Nuclear Society, 1978.

6.10 S. L. Wu and M. C. Billone, "Development and Verification of Failure-Analysis Model for FBR Fuel-Element Cladding," Nucl. Eng. and Design, 88 (1985) 195-214.

6.11 F. C. Monkman and N. J. Grant, "An Empirical Relation Between Rupture Life and Minimum Creep Rate in Creep Rupture Tests," Proc. American Soc. for Testing Materials, 56, 593 (1956).

6.12 J. M. Kramer, Argonne National Laboratory, Private Communications, February 10, 1992.

6.13 U.S. NRC, "Standard Review Plan," NUREG-0800, July 1981.

7. EVALUATION OF 4S FUEL DESIGN

This section consists of two parts. The first part is a qualitative evaluation of the 4S design that provides assessment of the fuel design issues and how the design features are expected to enable the fuel to reach its full life in the reactor without compromising its integrity. The second part is a quantitative evaluation of the design that is based on the LIFE-METAL code and comparison to the design criteria discussed in the previous section. This part also includes a parametric study that evaluates the design at conditions that are much more extreme compared to the design conditions. Finally, a conclusion on the design evaluation is presented.

7.1 FUEL DESIGN FEATURES

As mentioned before and shown in Table 2.2., the 4S fuel design differs from the typical design used in EBR-II and FFTF in a number of aspects. Those include the long life of 30 years, the fuel length and width, in addition to operation at lower linear power and peak hot-spot clad temperature. The following is an evaluation of the impact of those differences and how the design parameters provide mitigation of any possible impact on the fuel performance.

7.1.1 Fuel Long Life

The most distinguishing feature of this fuel design is its long life of 30 years compared to the 1-3 year fuel lifetime in a typical fast reactor. The main impact of the long residence time of the fuel is expected to be on its cladding thermal creep, possible fuel cladding chemical interaction, and sodium corrosion at the outer surface of the cladding.

As mentioned before, thermal creep of HT-9 is a limiting factor in fuel design, especially at high cladding temperature. Clad exposure to stresses for a long period of time can enhance the thermal creep response of the cladding. However, this is not expected to be the case for this design because of the low fuel burnup and relatively low plenum temperature (609°C peak hot-spot clad temperature compared to 650°C in EBR-II). Low average burnup of about 3.4 at.% combined with plenum volume that is about 1.3 times the volume of the fuel leads to low stresses due to gas pressure. Thus, the primary loading mechanism on the cladding, that is, the plenum pressure, is reduced to values that are at least 1/3 of the value for the typical EBR-II fuel achieving 10 at.% at the end of life. Also, as shown in Figure 4.1, the majority of the release of fission gases to the plenum takes place between 1-2 at.% burnup, that is, the majority of the release of fission gases takes place after at least 1/3 (10 years) of the fuel lifetime. Finally, our calculations of the clad thermal creep, given the stress history and the clad loading and taking into account the possible clad thinning from FCCI, indicate that the total thermal creep strain remain very low and much less than the design limit of 1%. This shows that thermal creep under the 4S conditions and long residence time in the reactor is not expected to be a life-limiting factor.

Sodium corrosion is mainly due to oxygen content in the primary sodium of the reactor. 4S design targets oxygen content to be less than 3 ppm, which is comparable to its content in EBR-II. Some of the EBR-II blanket pins were exposed to sodium temperature and oxygen content that are similar to the 4S fuel, and resided in the reactor for about the same period of time. Those blanket pins did not exhibit any corrosion problem due to exposure to sodium. Although those pins are made of 316 stainless steel rather than HT9, the corrosion behavior is similar [7.1]. Based on the corrosion rates of ferritic steel similar to HT9, no significant corrosion is expected at the temperatures and target oxygen levels of the 4S reactor after 30 years of exposure.

The third phenomenon that can be affected by the long life characteristic of the 4S fuel is FCCI. The key factor that enhances FCCI is the fuel cladding contact temperature, which is highest at the top of the fuel column. However, at this top location, as shown in Figure 7.1, the burnup is the lowest, about 1.5 at.% at the end of the life. This burnup is lower than the burnup value at which the fuel is expected to come in contact with the cladding, as shown in Figure 7.1 [7.2]. (Note that the top section is not shown in the figure since it does not come in contact with the cladding.) This is consistent with the experimental data relating the fuel swelling rates to burnup, as shown in Figures 4.1 and 4.3, where the contact between the fuel and cladding does not take place until a burnup close to 2 at.%. Thus, it should take at least 10 years for the fuel to come in contact with the cladding, at the lower part of the fuel where the temperature is lower. At the top of the fuel where the temperature is highest, the fuel will come in contact with the cladding for only a short period of time (or not at all) by the end of life.

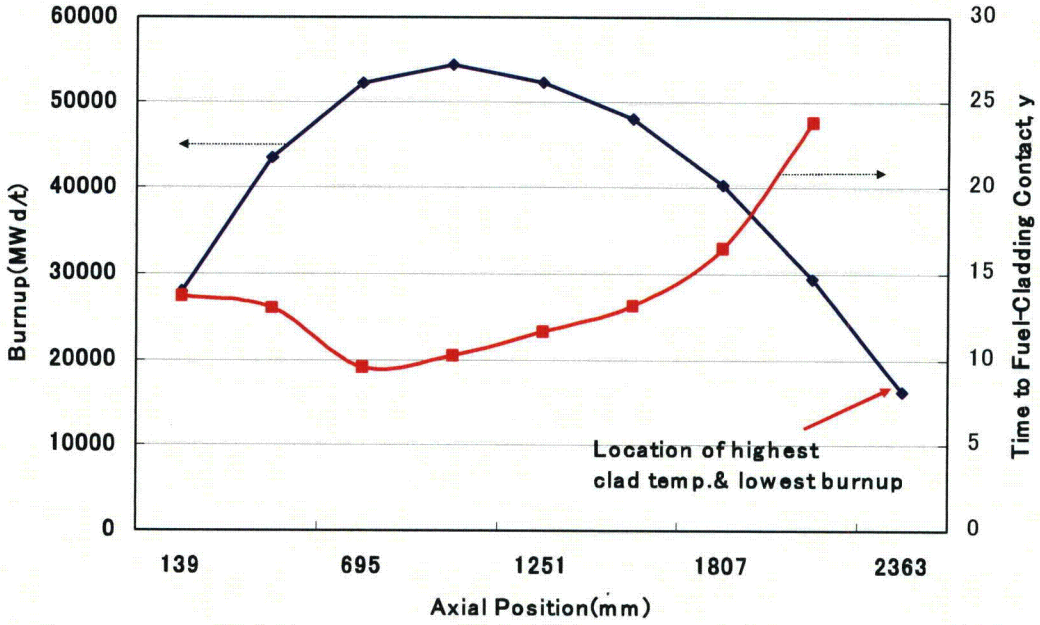

Figure 7.1. Axial Variations in Burnup and Contact Time between the Fuel and Cladding at the Different Axial Locations (from Ref. 7.2)

Complementary to this effect is the impact of the shape of the 4S power profile, in which the power peaking is shifted to the lower part of the fuel for most of the life of the pin compared to the power shape in EBR-II, as shown in Figure 7.2. As mentioned before, this power shape reduces the impact of FCCI as evidenced by PIE of the long metallic pins in FFTF, which has shown reduction in FCCI at the top region of the fuel (FFTF and 4S flux shapes are comparable). Finally, these facts combined with a relatively low cladding temperature, very low power at this location (source of rare earth, RE), and very low temperature gradient across the fuel (reducing the driving source for RE migration) undermine the effect of FCCI. As expected, calculations of FCCI penetration depth that are based on steady-state penetration depth correlations indicate that the cladding will maintain its integrity over the life of 30 years of operation.

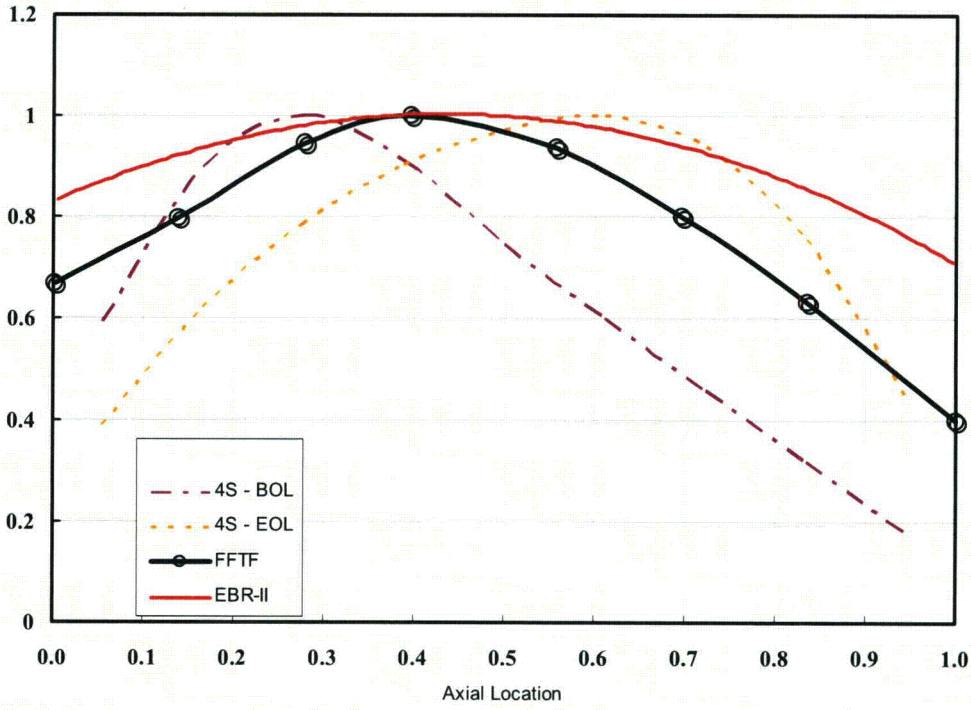

Figure 7.2. Comparison between the Axial Power Profiles of the 4S Reactor, EBR-II, and FFTF

7.1.2 Fuel Pin Diameter

Another characteristic of the 4S fuel is its large diameter, roughly twice the typical diameter of pins irradiated in EBR-II and FFTF. There has been experience with larger-diameter pins in EBR-II, however. There were specific experiments in EBR-II that tested larger-diameter pins similar to driver fuel to be used in commercial reactors [7.3] and advanced blanket fuel [7.4]. The experimental subassembly designated X430 [7.3] contained 37 pins with slug diameters of 5.71 mm, clad in HT9, which were larger than the typical 3.3 – 4.3 mm diameter EBR-II pins. These pins are still smaller than the

10.4 mm diameter 4S pins, however. Experiments X431 and X432 in EBR-II [7.4] were aimed at testing blanket U-Zr fuel. The slug diameter for these experiments was 7.95 mm. Measurements of axial fuel swelling, cladding diametral strain, and fission gas release for experiments X430, X431, and X432 indicated that the performance of these larger-diameter fuel elements is consistent with previous post-irradiation data for smaller diameters. In addition, there is experience with EBR-II blanket fuel with a diameter similar to that of the 4S fuel [7.5]. The performance of those wider-diameter pins did not differ signficantly from the typical EBR-II or FFTF pins. Thus, in general, no special effect is expected due to the increased fuel pin diameter of the 4S fuel.

7.1.3 Fuel Length

The 4S fuel slug length is characteristically longer than any driver pins irradiated in EBR-II or any other existing fast reactor, including Super-Phenix in France. Thus, there are no experimental data that correspond to such a long fuel slug design. Experience from the extrapolation of irradiation performance data from short fuel pins to long fuel pins exists, however. Long metallic fuel pins (36 inches compared to 13.5-inch EBR-II pins), about the same diameter as the EBR-II pins, have been irradiated in FFTF [7.6, 7.7]. Irradiation of these pins was in support of the IFR program and the effort that started in the late 1980s to convert FFTF from mixed oxide (MOX) fuel to metallic fuel.

The IFR-1 experiment [7.7] was the first metal fuel test irradiated in FFTF. The post-irradiation data from this test constitute the important available data that address the issue of the short pins database extrapolation to long fuel pins. The test consisted of 169 fuel pins: 18 with U-19wt.%Pu-10wt.%Zr fuel, 19 with U-8wt.%Pu-10wt.%Zr fuel, and the remainder of pins contained U-10Zr. The cladding for all pins was 20% cold-worked D9 cladding, the fuel smeared density was 75%, and the plenum/fuel volume ratio of the pins was 1.0. The diameter of the fuel was 4.98 mm. The pins were irradiated to a peak burnup of 10 at.% (fast fluence was 15.6×10^{22} n/cm^2). The peak burnup at the beginning of life ranged from 44 to 48 kW/m. The power shape over the pins is a chopped cosine with power at the bottom and top of the pins that is 50% lower than that at the middle. The above IFR-1 pin parameters show similarity with the EBR-II pins except for the fuel length (about 3 times longer) and the power shape (higher gradient in FFTF).

The main fuel stability concerns related to having a core with a long fuel column is that the increased height and weight of the column would cause fuel compaction or impeded fission-gas release. Fuel compaction can lead to enhanced localized fuel cladding mechanical interaction (FCMI). Impeded fission gas release can also lead to enhanced FCMI from increased fuel swelling. Post-irradiation examinations of a fraction of the test pins did not show signs of fuel instability. Those examinations included post-irradiation neutron radiography, axial gamma scanning, clad strain measurements, and fission-gas release measurements. Radiographic testing of 18 of the pins with different Pu contents (0, 8, and 19 wt.% Pu) showed axial fuel elongation that is consistent with the axial elongation of the pins irradiated at EBR-II. This is shown in Figure 4.3 (the

solid data points in the figure), where the average axial elongation is just slightly lower than the corresponding EBR-II data. Both radiographic and gamma scan data have shown that the axial fissile distribution within the fuel is uniform (except at the top where the fuel has lower density as it has more freedom to expand). None of the pins examined showed signs of local fuel compaction. Another sign of the absence of local compaction was apparent from the cladding deformation examinations. None of the pins examined has shown anomalous strain peaks that would suggest enhanced localized FCMI from fuel relocation. Finally, the fission-gas release fraction measured for one of the irradiated pins, 72%, was consistent with the EBR-II database (63% – 78%) for comparable fuel at 10 at.% burnup. Thus, the data indicated that the longer fuel column did not impede the release of fission gas from the fuel. Based on this discussion, the irradiation behavior of the full-length IFR-1 fuel pins was comparable to that of shorter EBR-II pins. The absence of a trend that shows even the slightest reduction in the IFR-1 fuel performance compared to the EBR-II fuel performance suggests that extrapolation of the EBR-II fuel behavior to the behavior of the even longer 4S pins will be achieved without performance reduction. Another point that supports the performance of the full-length commercial pins is that no failures were observed in any of the other six full-length metallic fuel experiments that were completed in FFTF (MFF series). The metallic pins in those experiments consisted of binary U-10 at.% Zr fuel clad in HT9 and many of those pins were exposed to more aggressive conditions than those of the IFR-1 pins. All have attained peak burnups exceeding 16 at.%.

The power peaking in the commercial reactor designs such as the 4S is expected to be different from the EBR-II power profile. As shown in Figure 7.2, the EBR-II power profile is flatter with a peak-to-average power over the pin of about 1.2, compared to a peak-to-average value of about 1.5 for the 4S design. The FFTF power shape is similar to the 4S power shape with a peak-to-average power value of about 1.5. This power shape did not seem to have any effect on the IFR-1 metallic pins behavior compared to similar pins irradiated in EBR-II. Thus, it is possible that the power shape in the proposed 4S design will not have much effect on the behavior of the metallic fuel compared to the behavior of the pins that constitute the EBR-II database. Finally, the performance of the long, 1.5-meter, EBR-II, discussed in the following section, is another indication that the long metallic fuel pin behavior in the 4S reactor is not expected to differ from past experience.

7.1.4 EBR-II Blanket Performance

EBR-II blanket fuel performance provides an indication of how the 4S fuel will perform over the 30-year lifetime in a fast reactor irradiation environment. Some of the blanket subassemblies remained in EBR-II core for the full life of about 29 years, which is about the same as the 4S fuel [7.8]. Although the depleted uranium blanket rods have very low power up to about 4.3 kW/m, this power is comparable to peak 4S power of about 8 kW/m, and about the same as the power at the top location of the fuel, which is the main location of interest where the clad temperature is the highest. The peak clad temperature of the blanket pins is about 600°C, which is nearly the same as the 4S clad.

The blanket fuel length is about 1.5 meters compared to the 4S's 2.5 meters. While the 4S fuel has 78% smeared density and a plenum length that is the same as the fuel length, EBR-II blanket fuel has a more restrictive 85-90% smeared density and a very short plenum region. Finally, examinations of blanket pins have shown no evidence of significant clad corrosion or FCCI [7.9].

7.2. LIFE-METAL EVALUATION OF THE 4S FUEL DESIGN

7.2.1 Input Parameters and Assumptions

Tables 2.2 and 2.2 include the important parameters used as input to the LIFE-METAL code for the evaluation of the current U-10Zr 4S fuel design. The power profiles over the life of the fuel are assumed to be the same as those shown in Figure 2.4. The BOL profile is assumed to be effective from the reactor startup until about 6.3 years. Between 6.3 years and 22 years, the MOL profile is used (average of the two profiles with and without full absorber), and the EOL profile is used between 22 years and the end of life of about 30 years. Although the power profile changes with time, the average pin power is maintained at 39 W/cm, while the peak pin powers go down and shift in location with time.

The average fast fluence is 1.9×10^{23} n/cm^2 > 0.1 MeV, which provides an average flux of 2.1×10^{14} n/cm^{2}s > 0.1 MeV over the 30 years of irradiation. In addition, the inner cladding temperature is assumed to be fixed during the simulation and to vary linearly from a value about the same as the inlet flow temperature at the bottom to a peak value at the top of the fuel. The peak inner cladding temperature is assumed to be 600°C for the base case, and goes up to 609°C when the hot channel factors are included (the peak nominal cladding temperature is about 567°C). Other general assumptions are as follows:

- No radial variation in power generation within the fuel.
- No radial redistribution of the fuel constituents.
- Plenum temperature is assumed to be the same as the flow outlet temperature.
- Fraction of sodium volume outside the fuel slug (it is assumed that Na fills the gap between the fuel and cladding) is equal to 1, i.e., no sodium logging.
- Fuel axial locking effects are not taken into account. This is a result of the simplifications made in the mechanical analysis modules of the code.
- Fuel enrichment is assumed to be 19 wt.%U-235.

7.2.2 Design Evaluation

As discussed in previous sections, the low burnup 4S fuel design with the appropriate smeared density of 78% (within the acceptable range of 75-80%) eliminates the possibility of fuel cladding mechanical interaction. This simplifies the loading mechanism on the cladding to that associated with the fission gas pressure. The stresses on the cladding increase with time due to the accumulation of fission gases and the possible reduction in cladding thickness due to FCCI and sodium corrosion of the cladding outer surface. Thus, given this simplification of the problem and before introducing the LIFE-METAL detailed calculations, it is possible to get a rough estimate of the bounding case for the 4S fuel as follows.

The design criteria discussed before are mainly concerned with the thermal creep component of clad strain, the hoop stresses on the cladding, and the CDF estimates. The temperature-related criteria are satisfied given the lower power and peak hot-spot clad temperature of the fuel. Thermal creep correlations of HT9 are available [7.10], and the stress calculations are straightforward given the fact that the cladding loading mechanism is the gas pressure. The fission gas generation in a 4S fuel pin is almost linear with time; the total amount of fission gas generated after average burnup of 4 at.% in U-10Zr fuel with 19% U235 enrichment is about 135 moles. The gas pressure is calculated to be about 3 MPa, assuming about 30% uniform fuel volumetric growth (closing the fuel-cladding gap uniformly, which is an overestimate of fuel swelling given the EOL burnup), and plenum temperature of 540°C (hot channel temperature), and 75% fission gas release from the fuel to the plenum (see Figure 4.1). Taking into account an assumed 20% reduction in the cladding thickness due to sodium corrosion and FCCI, the peak hoop stresses on the cladding due to gas pressure is < 30 MPa (<< 150 MPa limit) at EOL. At the location of the hottest cladding temperature (top of the fuel slug), and using HT9 thermal creep and stress rupture correlations, the calculated CDF is $< 10^{-4}$ and the thermal creep strain remains below 1%. Thus, an approximate, though representative, evaluation of the 4S fuel performance shows that the fuel will not violate the design criteria.

As mentioned before, the LIFE-METAL calculations represent bounding calculations for the 4S fuel performance since 30 years of actual irradiation data are not available for validating the code. However, the validation data used during the IFR program represent more severe operating conditions and provide a sort of conservatism to the evaluation of the 4S fuel performance. The current version of the code was validated and frozen at the end of the IFR program and was used in EBR-II Mk-V fuel evaluation [7.11, 7.12, 7.13]. The U-10Zr/HT9 fuel settings were used, and the 4S input data shown in previous section were used (calculations at 4 at.% average burnup instead of 3.6 at.% for conservatism). No alterations to this version of the code were made and no changes to the model parameters, such as the gas release and wastage, were made. The results of the evaluation show that **none of the design criteria for this 4S design are violated by the end of the 30-year lifetime**. At the location of interest, the top of fuel where the cladding temperature is highest, the calculated CDF is about 3×10^{-4}, and the thermal creep strain is about 0.2%. The contact between the fuel

and the cladding at the top of the fuel took place very late in the life of the pin, after about 23 years of operation, causing a relatively small amount of FCCI by the EOL. The fission gas release fraction resulting in those calculations was more than 85%, which is higher than what will be expected during operation, given the low average burnup of the pin. This high gas release provides another level of conservatism since it leads to higher plenum gas pressure and higher hoop stresses on the cladding, although this hoop stress, at about 20 MPa, remains much less than the design criterion of 150 MPa.

7.3 SURVEY ANALYSIS OF THE 4S FUEL PERFORMANCE

This section describes a parametric study of the limiting cases for the 4S fuel design. Those cases are intended to show the viability of the design in terms of performance at extreme conditions to which this fuel design is unlikely to be subjected. For example, extreme cases include cladding temperatures higher than the hot-spot temperature, high fuel swelling rate that leads to early fuel-cladding contact at locations of low burnup/high temperatures, and FCMI at location of peak burnup. Associated with the high radial fuel growth is a fission gas release fraction of about 50%, which was achieved for all cases. Finally, increasing fuel burnup increases the fission gas pressure and enhances all other phenomena that represent loading on the cladding. The high peak clad temperature and early fuel-cladding contact at the location of high temperature enhances the wastage due to FCCI and enhances thermal creep strain. As mentioned before, the peak cladding temperature parameter and fuel burnup profiles are input to the LIFE-METAL code, so it is directly increased in the input file to achieve the desired value. The fuel swelling increase is achieved through altering the coefficients of the correlation for the fission gas release and fuel swelling. This alteration leads to early contact (after only about 3 years of operation) between the fuel and the cladding at the top of the fuel column where the cladding temperature is highest. Table 7.1 provides the temperature and burnup combinations at which the parametric study was performed, where the inner clad temperature ranged from 609° to 630°C and the fuel average burnup ranged from 3.6 to 4.5 at.%.

Table 7.1. Survey Analysis List of Conditions

	Average Burnup		
Peak Clad Temp., °C	**3.5 at.%**	**4.0 at.%**	**4.5 at.%**
609	*case0*		*case2*
620		*case1*	*case3*
630		*case4*	

Given a new value of peak cladding temperature, the linear distribution of clad temperature used as input to the LIFE-METAL code is altered so that the peak clad temperature at the top of the fuel location is the same as the new value and proportionally increases the other temperatures. To increase the burnup while maintaining the same flux

shape, the average linear power is increased proportionally to the change in burnup compared to the original case. Also, the flux values are changed proportionally to the change in burnup.

Table 7.2 is a summary of the key EOL evaluation parameters for all the cases and their comparison to the design criteria. As shown in the table, no design criterion is violated. The thermal component of cladding creep is much lower than the 1% limit, the CDF is much less than the 0.05 value, and the hoop stresses are less than the 150 MPa limit (the fuel temperature limits are also met). Note that the results shown in the table include degradation in cladding thickness due to FCCI and sodium corrosion that reaches as much as roughly 50% of the as-fabricated cladding thickness at the top of the fuel. This degradation in the cladding thickness did not lead to violations of the design criteria, however, especially thermal creep, and the thick cladding was able to accommodate the degradation and accumulated stresses.

Table 7.2. Survey Analysis Results for the Different Cases

Operating Conditions		**Thermal Creep Strain, %**	**CDF**	**Hoop Stress (gas pressure), MPa**
Peak Clad T, °C	**Burnup, at.%**			
609	3.6	0.1	9.0E-06	15
609	4.5	0.16	6.0E-5	20
620	4.0	0.3	2.0E-4	20
620	4.5	0.43	5E-4	22.4
630	4.0	0.82	1.0E-3	23.5

7.4 CONCLUSIONS

The current 4S fuel design is based on U-10Zr metallic fuel with extended irradiation data from EBR-II and FFTF, in addition to a database of out-pile experiments. Based on the discussion in the previous evaluation sections, it is concluded that this design is viable and will be able to accommodate the long period of irradiation in the reactor. This is achieved through the use of milder operating conditions that compensate for the effects of the long irradiation period, and the enhanced physical characteristics of the fuel pins compared to EBR-II and FFTF fuel. The linear power is very low, less than 20% of EBR-II or FFTF linear powers, and the cladding thickness is about twice that of the cladding used in those reactors. The fuel diameter is also about twice that of EBR-II and FFTF fuel. In addition, the peaking of the power distribution in the lower part of the fuel during most of the irradiation period also helps the fuel durability, as the highest fission rates (RE generation rate) take place in the colder part of the fuel. All these fuel features, combined with the irradiation experience of the blanket fuel in EBR-II, make

the case that 4S fuel is expected to perform adequately over its long life of 30 years. A quantitative evaluation of the fuel performance using the LIFE-METAL code also confirms this conclusion and shows that the 4S design meets a set of conservative pre-specified fuel integrity design criteria. Those criteria are found to be met even under conditions that are more severe than the expected conditions in the reactor. Finally, it is possible to state that, based on the experimental database and fuel performance code assessments, 4S fuel is expected to perform adequately during normal operating conditions.

REFERENCES 7

7.1 K. Natesan, private communications, Argonne National Laboratory, December 2007.

7.2 Y. S. Kim, A. M. Yacout, G. L. Hofman, and H. J. Ryu, Trans. Am. Nucl. Soc., Vol. 96, p. 709, 2007.

7.3 D. C. Crawford, S. L. Hayes, and R. G. Pahl, "Large-Diameter, High-Plutonium Metallic Fuel Testing in EBR-II," Trans. Am. Nucl. Soc., 71, 178 (1994).

7.4 R. G. Pahl, et al., "Irradiation Behavior of Metallic Fast Reactor Fuels," Journal of Nuclear Materials, 188, (1992) p. 3-9.

7.5 R. D. Leggett and L. C. Walters, Status of LMR Fuel Development in the United States of America, Journal of Nuclear Materials, **204**, (1993) pp. 23-32.1.2.

7.6 A. L. Pitner and R. B. Baker, "Metal Fuel Test Program in the FFTF," Journal of Nuclear Materials, 204, (1993) p. 124.

7.7 H. Tsai and L. A. Neimark, "Irradiation Performance of Full-Length Metallic IFR Fuels," Proceedings of the International Conference on Design and Safety of Advanced Nuclear Power Plants (ANP'92), Vol. III, 23.2-1, 1992.

7.8 D. Porter, Idaho National Laboratory, private communications, 2007.

7.9 L. C. Walters, B. R. Seidel, and J. H. Kittel, "Performance of Metallic Fuels and Blankets in Liquid-Metal Fast Breeder Reactors," Nuclear Technology, 65, (1984) pp. 179-231.

7.10 Ho Jen et al., submitted to Journal of Nuclear Materials, 2008.

7.11 L. Briggs, et al., private communications, March 1995.

7.12 L. K. Chang, D. J. Hill, and J. Y. Ku, "A Method for the Determination of Technical Specifications Limiting Temperatures in EBR-II Operation," Fourth International Topical Meeting on Nuclear Thermal Hydraulics Operation and Safety, April 5-8, 1994, Taipei, Taiwan, R.O.C.

7.13 Integral Fast Reactor Program Annual Progress Report, FY 1993, ANL-IFR-244.